SIMULATED SYNOPTIC VARIABILITY AND STORM TRACKS OVER NORTH AMERICA AT THE LAST GLACIAL MAXIMUM

by

ROBERT PAWLAK

A thesis submitted to the

School of Graduate Studies

Rutgers, The State University of New Jersey

in partial fulfillment of the requirements

for the degree of

Master of Science

Graduate Program in Atmospheric Science

written under the direction of

Dr. Anthony J. Broccoli

and approved by

_____

_____

_____

New Brunswick, New Jersey

JANUARY 2018

ABSTRACT OF THE THESIS

Simulated Synoptic Variability and Storm Tracks Over North America at the Last Glacial Maximum

by ROBERT PAWLAK

Thesis Director:

Dr. Anthony J. Broccoli

Transient eddy activity over North America during a simulated Last Glacial Maximum (LGM) is modeled by measuring synoptic variability, Eady growth rate, and comparing daily time series distribution plots of 2-m reference temperatures. The role of transient eddies in the climate, south of the Laurentide Ice Sheet (LIS), is not well understood. Quantifying changes to transient eddy activity will assist future climate modelers who wish to simulate the climate of an ice sheet terminating in a continental interior at the mid-latitudes. A band pass temporal filter is used to isolate synoptic scale variability in a simulated LGM climate using the Geophysical Fluid Dynamics Laboratory (GFDL) coupled atmospheric-ocean general circulation model CM2.1 for both January and July. LGM climate is simulated using orbital parameters, greenhouse gas concentrations, and sea level values set to 21,000 years before present and the ICE-5G ice sheet reconstruction used as climate forcings. A control run used pre-industrial (PI) values for comparison. Maximum Eady growth rate is used to quantify baroclinic wave growth of transient eddies. Transient eddy activity is suppressed over LIS in January. Increased activity is

concentrated along the coastline of the Gulf of Mexico and the east coast of North America. In July, this increased transient eddy activity is found over the unglaciated landmass south of the ice sheet where it is less prevalent in the control run. Frequency distributions of daily 2-m reference temperatures depict warming events south of the ice that are likely associated with transient eddies in both January and July. In July, there is a notable increase of these events compared to PI.

TABLE OF CONTENTS

ACKNOWLEDGEMENTS

I would like to thank my faculty advisor, Dr. Anthony Broccoli. His mentorship allowed me to mature on an academic and personal level. I could not have progressed through this research during the recent wonderful and tragic events of my life without his advice and support.

I would also like to thank the committee members of the thesis. Dr. Benjamin Lintner who provided invaluable academic advice and Dr. Steven Decker.

I would like to thank Dr. Bryan Raney who had the patience to teach me how to code from scratch as well as providing technical support. Huge thanks go out to Max Pike, Joe Slezak, Sarah Tannenbaum and the rest of the graduate students that I came to know.

I would also like to thank my wife Valentina who provided me the support I needed at home to get through my schoolwork.

DEDICATION

To my wonderful daughters Verene and Athena.

One of whom provided many sleepless nights.

LIST OF TABLES

LIST OF FIGURES

1 INTRODUCTION

This thesis attempts to quantify the changes in synoptic variability over North America at the Last Glacial Maximum (LGM), approximately 21,000 years before present. There is an emphasis on the effects of the presence of the Laurentide Ice Sheet, which at its maximum extent covered a large portion of the North American landmass. Changes in orbital parameters, or Milankovitch cycles (Berger, 1988), provide the necessary climate forcing to trigger the LGM. Forced climate cooling require both sensible and latent heat from the lower latitudes to be transported poleward to balance the global energy budget (Lorenz, 1979). Mid latitude cyclones form to transport energy poleward and upward (Eady, 1949) to balance radiative cooling where an equator-pole overturning circulation cannot establish on a rotating Earth. The motion and structure of these cyclones are dictated by meridional temperature gradients and the zonal flow (Charney, 1947). The presence of an ice sheet spread over half of North America and of several kilometers thickness modifies the temperature gradient and presents a topographical barrier (CLIMAP, 1976). Although there is a lowered global mean radiative forcing, mainly due to increased albedo provided by the ice sheets and a lowered CO_2 concentration, tropical cooling is moderate. The temperature gradient over the mid latitudes is steeper.

The present-day temperature gradient did not simply migrate South due to an extended region of polar air. The Hadley cell dominates the energy transport from the tropics into the mid-latitudes which is weaker in the LGM along with an increase of polar subsidence (Gates, 1976). Observations depict a narrowing of the temperature gradient south of the ice sheet. Enhanced baroclinicity along the ice sheet edge modifies migratory cyclones controlling ice sheet expansion (Manabe and Broccoli, 1985). Thermal wind establishes itself perpendicular to

this temperature gradient and is a driving force for baroclinic instability (Charney, 1947). Since thermal wind is a vertical shear of geostrophic wind, it balances differences in horizontal gradients of layer-mean temperatures. As this gradient deepens as in the LGM, so must this vertical shear.

Deviations from the zonal mean flow, known as stationary waves, are created as moving columns of air act to conserve potential vorticity due to changes of relative vorticity, planetary vorticity, and column depth (Rossby, 1939). Topographical barriers reduce the column depth creating curvatures in flow. In westerly flow, air columns deflect to the north approaching a barrier creating a cyclonic curvature. Downstream of the barrier, an anticyclonic curvature develops when air columns deflect to the south to conserve potential vorticity. The LIS topography enhances the stationary Rossby wave induced by the Rocky Mountains and tilts its orientation to the northeast (Manabe and Broccoli, 1985; Kutzbach and Guetter, 1986; Justino et al., 2005). The blocking situation upstream of the ice sheet splits the mean flow over Western North America which is most notable in winter. The Northern branch of the flow extends over most of Canada while the Southern branch follows a zonal orientation over the Southern United States. The convergence of these branches strengthens to Polar Jet as is enters the Atlantic Ocean. During summer, the polar jet is simulated over the southern flank of the ice sheet which is representative of the thermal wind. A similar, but smaller ridge appears upstream of the Eurasian Ice Sheet over Western Europe.

The term “storm tracks” is used in the thesis as it is widely used in literature. Storm tracks are the areas of maximum variance on the synoptic time scale of mid tropospheric geopotential heights, typically the 500 hPa level. In this case, the storm tracks are a phenomenon that occur along a nearly zonal band across an ocean. The storm track entrance is an interface between a cold continental coast and a warm Western ocean current that is also

intersected by the polar jet. The storm track exit is located near the Western coast of a continent where cyclone kinetic energy is barotropically converted.

Storms naturally occur outside of these storm tracks and as this thesis is focused on variability over North America, another metric is used. Transient eddies are synonymous with mid-latitude storms and geopotential variance at the 500 hPa level is a measure of transient eddy activity. High variance of these heights is indicative of stronger or more prevalent occurrences of transient eddies. The term “transient eddy activity” is used to described this. The term “cyclone tracks” is used to describe the paths of individual cyclones. The application of temporal filters to isolate the contributions of the synoptic time scale are used to great effect to describe the structure of the oceanic storm tracks present in the LGM (Justino et al., 2005; Li and Battisti, 2008; Laine et al.,2008; Donohue and Battisti, 2009). Synoptic variability over the continental areas of North America does not receive as much attention.

In this thesis, we present the case that the presence of the LIS at the LGM concentrates synoptic variability within a relatively narrow corridor on the southern flank and downstream of the ice sheet. This region has enhanced baroclinic instability due to the changes in topography and upper level flow. Transient eddies develop rapidly within this corridor which serves as the storm track entrance for the North Atlantic. As for the North American landmass, the LIS suppresses transient eddy activity over much of the continent during winter. Unlike present day, transient eddy activity has a relatively larger role in heat and moisture transport during summer.

2 MODEL AND METHODOLOGY

2.1 MODEL

This study uses the GFDL CM2.1 global coupled climate model. While a detailed discussion of this model is provided in Delworth et al. (2006), here a few brief remarks about the model and its operation are provided.

GFDL's Flexible Modeling System's coupler calculates radiative fluxes between land, atmosphere, sea ice, and ocean components and no flux adjustments are used. The land and atmosphere resolution is 2° latitude x 2.5° longitude. The atmospheric model has 24 vertical layers and uses a 3-hour time step for radiation and 30-minute time steps for other physics including the diurnal cycle of insolation. Radiative effects of greenhouse gasses (GHGs) and a limited selection of aerosols including black carbon, organic carbon, sulfates, sea salt, and dust are included. The land model contains ten different land surface and vegetation types which are prescribed. The LGM simulation is set to have the same distribution of land surface and vegetation as in the control except where there is an ice sheet or an exposed sea floor due to the prescribed lower sea level. The land model collects runoff in a river's drainage basin and transports it to the river mouth where freshwater fluxes into the oceans are calculated. Ocean model resolution is 1° x 1° and becomes progressively finer equatorward of 30° to a resolution of 1/3° at the equator. It has 50 vertical layers with 22 10-m thick layers in the top 220 m. It uses a 2-hour time step. The sea ice model includes three vertical layers, one of which is snow, and five thickness categories, accounting for internal stresses and thermodynamics. Flux exchanges between the different components are calculated on the ocean model time step of 2 hours.

We compare two different runs of CM2.1. The first is a preindustrial (PI) experiment used as the control run. Boundary conditions for the control run uses modern day ice sheets, topography, coastlines, and orbital parameters. GHG concentrations from the year 1750 are used, including 280 ppm CO_2, 760 ppb CH_4, 270 ppb N_2O, no CFCs, and modern minus 10 dobson units (DU) for O_3. One DU is equivalent to 0.01 mm thickness of pure 0_3. The second is a simulated LGM. It uses the Paleoclimate Modelling Intercomparison Project Phase 2 (PMIP2) reconstruction of the ice sheets based on ICE-5G reconstruction of the ice sheets (Peltier, 2004). The boundary conditions for the LGM run are abruptly introduced. Ice sheets, topography, and coastlines are used from the ICE-5G data set. Global sea level is 125 m lower than the control. GHG concentrations are lower or the same: 185 ppm of CO_2, 350 ppb of CH_4, 200 ppb of N_2O, while the same values for CFCs and O_3 are used. Ocean salinity was simulated as having one practical salinity unit higher globally relative to PI. The solar constant is the same for both runs and orbital parameters are nearly identical. The model is run with 1400 years of simulated time where the PI experiment is contained. At year 1400, LGM boundary conditions are applied. The LGM run stops after 3600 years of additional simulated time when the drift of surface air cooling per century became relatively small. This drift is less than 0.03 K per century and is still present in the simulation. The last 100 years are used for this thesis.

2.2 METHODOLOGY

Output from these simulations are analyzed in the form of climatological averages and daily time series, focusing on January and July as indicative of winter and summer conditions. To examine variability on synoptic time scales, we apply a band pass filter (BPF) based on the work of Blackmon (1976) to the time series to certain variables. We want to address the effect of synoptic time scales of 3-7 days on variability. The coefficient values for a 21-point filter used by

Blackmon and Lau (1980) as shown in Table 2.2.1 are found to be acceptable. To accomplish this, we apply a weighting function on each time series variable.

$$\hat{x}_i = \sum_{i=-10}^{10} a_i \, x_i \qquad (1)$$

a_i represents the weighting coefficient, x_i is the unfiltered variable within the series and $\hat{x}_i$ is the variable with the filter applied. Constraints are applied so that only the North American quadrant is the output to save computing time. The filter successfully removes the effect of higher and lower frequency time scales on the filtered time series. Afterwards, the BPF time series is sorted into monthly categories so that January and July could be analyzed.

Weighting Coefficient	Bandpass Filter Value
α_0	0.4522054510
α_1	-0.0728693709
α_2	-0.2885051308
α_3	0.0973270826
α_4	0.0395130908
α_5	0.0283273699
α_6	0.0331625327
α_7	-0.0708879974
α_8	-0.0022652475
α_9	0.0030189695
α_{10}	0.0070759754

Table 0.2.1: Coefficient values used for weighting function in 21-point temporal filter. Values used are the same as in Blackmon and Lau (1980).

Given our interest in how synoptic scale circulations differed during the LGM, we consider the Eady (1949) model for baroclinic instability. Following Eady (1949), Maximum Eady growth rate σ is calculated according to the following formula:

$$\sigma = 0.3098|f|\frac{|\frac{\partial u}{\partial z}|}{N} \quad (2)$$

where f is Coriolis parameter, $\partial u/\partial z$ is vertical wind shear, and N is the static stability. The constant comes from the most unstable mode of the Eady growth rate (Lindzen and Farrell, 1980). This is based on the Rossby radius of deformation where the ratio of the horizontal length scale is 100 :1 compared to the vertical scale. Using typical values for the variables in the Eady model, the most rapid rate of unstable growth occurs using a constant of 0.3098.

Vertical wind shear is calculated using the difference of zonal winds u and heights z from one pressure level p above and below.

$$\frac{\partial u_p}{\partial z_p} = \frac{u_{p+1} - u_{p-1}}{z_{p+1} - z_{p-1}} \quad (3)$$

This potential temperature θ is calculated using Poisson's equation where temperature is T, P_0 is 1000 mb, P is the pressure, R is the universal gas constant, and c_p is the specific heat at constant pressure.

$$\theta = T\left(\frac{P_0}{P}\right)^{\frac{R}{c_p}} \quad (4)$$

The static stability term is calculated using the Brunt-Vaisala frequency. Brunt-Vaisala frequency is calculated using gravity and potential temperature as well as the change of potential temperature with height:

$$N = \left[\frac{g}{\theta_p}\left(\frac{\theta_{p+1} - \theta_{p-1}}{z_{p+1} - z_{p-1}}\right)\right]^{1/2} \quad (5)$$

The Coriolis parameter f is calculated by multiplying twice the rotation rate of the Earth Ω, by the sine of latitude $\emptyset$.

$$f = 2\Omega\sin(\emptyset) \quad (6)$$

After finding the Eady growth rate, the individual terms of vertical shear and static stability are investigated to find the dominant contributor.

Thermal wind is also shown in another representation to depict the tropospheric column. It is calculated by taking the absolute value of the differences of the 200 mb zonal wind component and the surface wind component divided by the 200 mb heights subtracted by the elevation. Being in the mid-latitudes and using monthly zonal mean wind components, the atmospheric profile is approximated to be nearly geostrophic. The thermal wind is a representation of the vertical shear of zonal geostrophic winds.

$$\frac{\Delta u}{\Delta z} = \frac{u_{200mb} - u_{sfc}}{z_{200mb} - z_{sfc}} \quad (7)$$

Animations are produced using a combination of SLP, precipitation, and temperature charts as snapshots of one day as part of a slide show. An arbitrary 10-year long segment from four different regimes is chosen to demonstrate transient eddy propagation within each regime.

The regimes mentioned are January LGM, July LGM, January PI, and July PI. The length of time is chosen to provide at least three minutes of viewing time to reasonable analysis. It provides a compromise between analyzing climate processes, computation time, and file sizes for archive. They include 3100 days in chronological order. The jumps between the end of month of the previous year and the beginning of the month of the following year needed to be accounted during any analysis.

3 RESULTS

Direct comparisons are made by computing anomalies of each variable in the LGM relative to PI.

3.1 TIME AVERAGED QUANTITIES

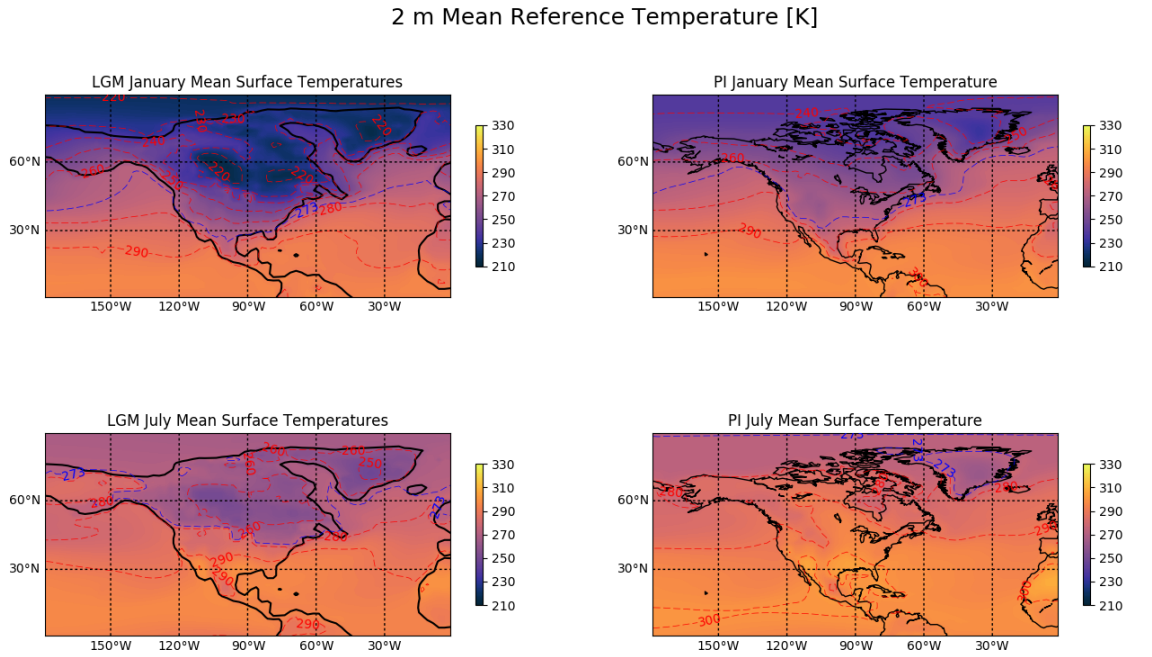

Figure 3.1.1: Mean monthly 2-m temperatures with contours at intervals of 10 K in red. The blue isotherm is the freezing isotherm. LGM coasts are representative of the estimated drop of sea level.

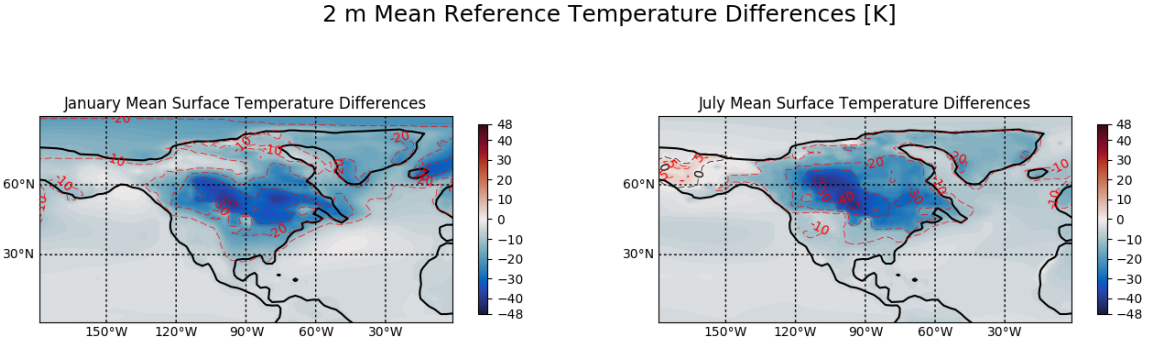

Figure 3.1.2: Mean monthly 2-m temperature differences between the LGM and PI. Contour intervals are measured at every 10 K below zero and at positive 5 K. LGM coasts are used for difference maps.

The entire North American region shows cooling in the lower troposphere during the LGM. Warming in Alaska in summer of up to 5 K is found where there is land in the LGM run and ocean in PI. Differences between LGM and PI during the winter and summer shows maximum cooling over the eastern portion of the ice sheet at most pressure levels. There is warming of up to 2.5 K at the 200 hPa level of over the eastern portion of the ice sheet and the entire Arctic Circle for the summer and at certain locations during winter. This is due to the lowered height of the tropopause. There are three notable areas of minimum 2-m reference temperatures which are easily distinguishable in Figure 3.1.1. In January, the mean temperature is under 220 K where elevations reach 4,000 m over the LIS and Greenland Ice Sheet. This is also reflected in Figure 3.1.2 for the LGM-PI difference in temperatures where maximum cooling occurs in those high elevation areas of the LIS. Over the max elevation of the LIS, the dry adiabatic lapse rate accounts for most of the cooling in January. In July, there is potentially up to 5 K of additional cooling. The exception is Greenland where an ice sheet existed in PI. In January, a strong temperature gradient forms south of the LIS over continental North America. The 290 K isotherm resides over the Gulf of Mexico for both runs. In PI, the 240 K isotherm nears the Arctic Circle where it resides between 45° N and 50° N for the LGM. There is also an equatorward shift of the freezing line. This is where anticyclonic circulation provided by the Laurentide High and katabatic winds supplies northerly flow of colder air as shown in Figure 3.1.3. The temperature gradient is only marginally stronger over the western Atlantic. It becomes progressively more pronounced toward the eastern Atlantic along the sea ice margin. In July, the enhanced temperature gradient is constrained to the southern margins of the ice sheets and the freezing line closely conforms to its shape. Katabatic winds are suppressed by intense diabatic heating and zonal flow is established. Freezing air over the ice sheet remains due to the high albedo characteristic reflecting the majority of incoming short-wave radiation and the inhibition of

sensible heating. The ice sheet surface cannot exceed freezing or else it will lose the solid characteristic of water. Thus, conduction and convection may raise the temperature of air parcels slightly above freezing with the presence of meltwater at the surface but it is at a negligibly small scale. Warm air advection as seen in time series plots and animations in later sections does not bring 2-m temperatures more than a few degrees above freezing and only on the southern fringes of the LIS. The cooling of 2-m temperatures in the North Atlantic associates with the outflow of polar air provided by the northern branch of the jet between the LIS and Greenland. This cooling decreases in July when this jet branch is weaker.

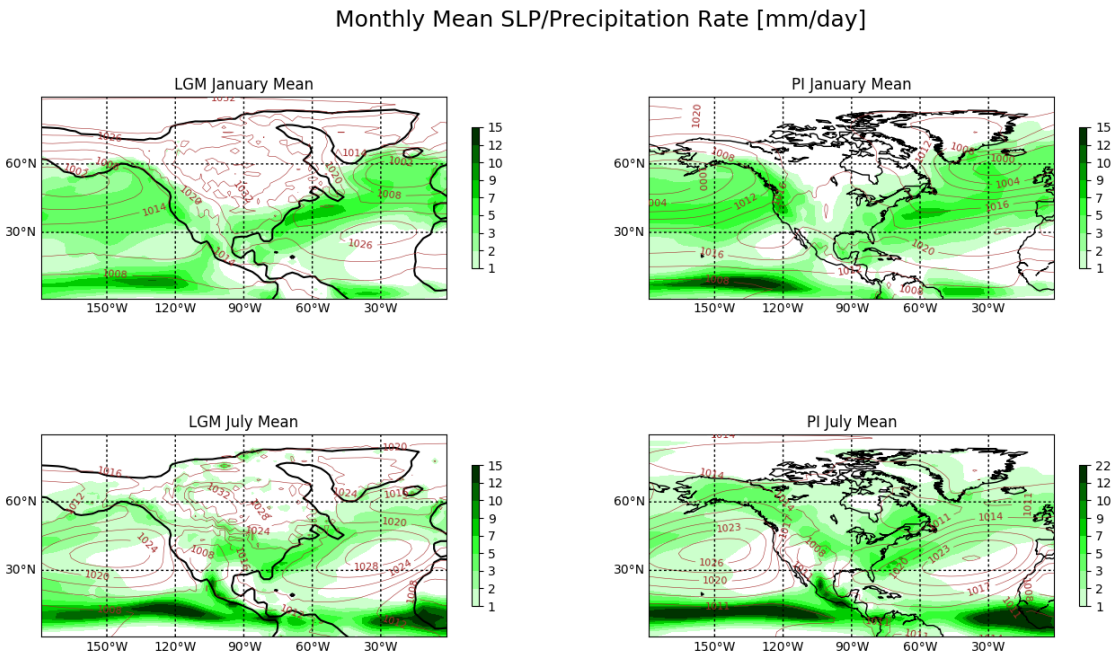

Figure 3.1.3: Monthly mean SLP in hPa and total precipitation rates in mm/day. Brown contours measure SLP. LGM SLP values are corrected to present PI representative values for direct comparison. Precipitation is shaded in green.

Sea level pressure (SLP) differences are calculated annually and for summer and winter after being corrected for ice sheet displacement. Global mean SLP in the LGM simulation is found to be 13.4 hPa higher than in the PI simulation due to the displacement of air and

decreased sea level due to the expanded ice sheets during the LGM. To better enable comparisons between the LGM and PI simulations, 13.4 hPa is subtracted from LGM SLP values.

Results show a 10 - 20 hPa increase over the ice sheet for each time period. Increases in SLP appear to the south of the ice sheet but are less pronounced in the summer. For winter, a maximum decrease of about 7 hPa is found in the middle of the Pacific storm track south of Beringia and notable decreases along the entire eastern portion of the track leading into the west coast, south of the Pacific Northwest. Beringia is the region encompassing present day Alaska and the exposed sea floor of the Bering Strait. A similar arrangement is found for the North Atlantic track with a smaller magnitude (<=5 hPa). An 8 hPa increase is found in the southern North Atlantic. In summer, the Pacific regime had a smaller difference from PI of about 1 hPa but is nearly identical. For the North Atlantic storm track, SLP decreases are nearly nonexistent. The high-pressure center in the subtropical North Atlantic migrates poleward. The southeastern US and Gulf of Mexico has a small decrease under 2 hPa as opposed to the increase in winter.

Migratory high and low-pressure regimes appear to oscillate between winter and summer in the Northern Atlantic and Pacific Oceans which is shown in Figure 3.1.3. A north-south orientation occurs in the Atlantic where increased SLP values appear in the northern portion during summer and vice versa in the winter. The Icelandic Low which deepens in winter experienced some filling in summer by an enhanced Azores High. Decreased values of SLP appear in the eastern North Pacific during winter and migrate west in summer. The Aleutian Low deepens, and the North Pacific High is weakened. The Great Basin High in the winter PI is replaced by the LIS High further to the North. Although, the LIS High remains as a permanent feature all year round. The North American Thermal Low that appears during PI summer as a monsoonal feature is also present in the LGM and is deeper. These SLP representations of semi-

permanent pressure systems reveal the reorganization of the general circulation in the middle to high latitudes over the North American region.

There are decreases to the mean and maxima of precipitation rates in the LGM which is to be expected due to the lower atmospheric water vapor content that is present. Due to the overall decrease of water vapor, global mean precipitation decreases. Differences of mean global mean annual precipitation show a decrease of 0.33 mm/day of total precipitation in the LGM simulation. Local changes in precipitation should be viewed within the context of an overall global decrease. Local decreases should be thought of as slightly exaggerated. Conversely, local increases should be given more weight due to having to overcome the obstacle of less water vapor content. The difference shows a southward shift of precipitation in the LGM run. The largest local decreases are over the ice sheet with a maximum decrease of 5 mm/day over present day Quebec. Precipitation increases for both seasons over the southern half of present day United States and follows the southwest to northeast tilted orientation of the east coast. A local maximum of 4-5 mm/day in the summer season is centered off the coast near the Gulf of Saint Lawrence. There is a decrease just to the south of the ice sheet extending to 36° N in the winter and further south to 31° N in the summer.

Figure 3.1.3 also shows the monthly mean precipitation rates for January and July. In PI January, precipitation is present along the entire west coast of North America except for the Baja coast with a large maximum of 10 mm/day near the Pacific Northwest. In the LGM, the North Pacific High weakens, and increased precipitation occurs over the North American Southwest. LGM precipitation does not extend as far inland as in PI. Figure 3.1.4 shows the differences between LGM and PI precipitation. As much as 4 mm/day decreases over the coast of the Pacific Northwest. These decreases continue upstream over the Gulf of Alaska. To the south, there are increases over the ocean and North American Southwest under 2 mm/day.

There is a minor decrease over the Gulf of Mexico and minor increases along the Gulf Stream and the sea ice margin halfway across the Atlantic. However, precipitation is prevalent in the North Atlantic in PI January. In the LGM there is significant precipitation along the sea ice and ice sheet margins which are well within the 2-m reference freezing isotherm. Maximum precipitation is found in the western portion of the Atlantic storm track. The central portion of the North Atlantic receives less precipitation due to the strengthened Azores High in the LGM. The parallel structure of increases and decreases over the Atlantic signifies an equatorward shift of the storm track.

In July, precipitation remains near the coasts of western North America due to the weakened North Pacific High in the LGM. Intrusion further inland occurs near the Pacific Northwest. Although there is less precipitation overall near Central America, there is increased advection toward the North American Southwest in the LGM. There are 2 mm/day increases over the Midwest and further north to 50th parallel which is well beyond the ice sheet margin. Other notable increases in excess of 2 mm/day are found over present day Florida, near the Gulf of Saint Lawrence, and the North Atlantic storm track exit region. Maximum decreases occur over the eastern portion of the LIS. Precipitation is scattered all over the LIS, especially along the southern margin. This is in stark contrast to January. There is hardly any precipitation over Greenland in either month.

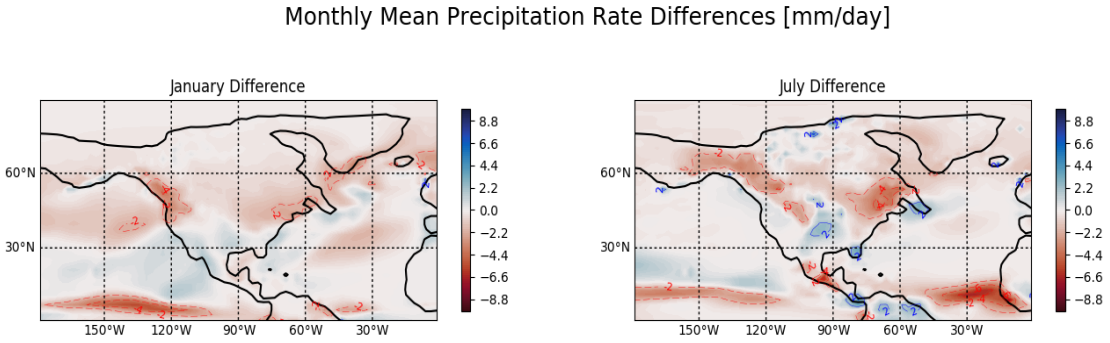

Figure 3.1.4: Monthly mean differences in total precipitation rate. Areas shaded in red and blue indicate lower and higher precipitation rates in the LGM, respectively. Contours are added at intervals of 2 mm/day.

A comparison of vector winds displays strengthened zonal mean flow at 500 hPa and 300 hPa over the mid-latitudes in the LGM in Figures 3.1.5 and 3.1.6. Over the west coast of North America, there is enhanced blocking in the mid and upper troposphere decelerating westerlies entering the Gulf of Alaska. To the south, there are clear placements of the mean jet over the oceanic storm tracks with maxima over the western portions. There are up to 20 m/s increases in these maxima in January. During LGM winter, there is a branch of strong winds between 15-20 m/s downstream of the ridge axis over the continental interior in the high latitudes. In figures 3.1.6 and 3.1.7, the northerly wind component from this region is strong and fed into the consolidated jet region on the eastern coast of North America. This is where the southerly component is strongest along with the maximum westerly component. This is indicative of poleward transport along the mean flow by developing eddies. The deceleration of the mean flow on the eastern side of the oceans and blocking on western continents are induced by topography. The jet core corresponded with the position of maximum precipitation and the tightest temperature gradient outside of the ice sheet.

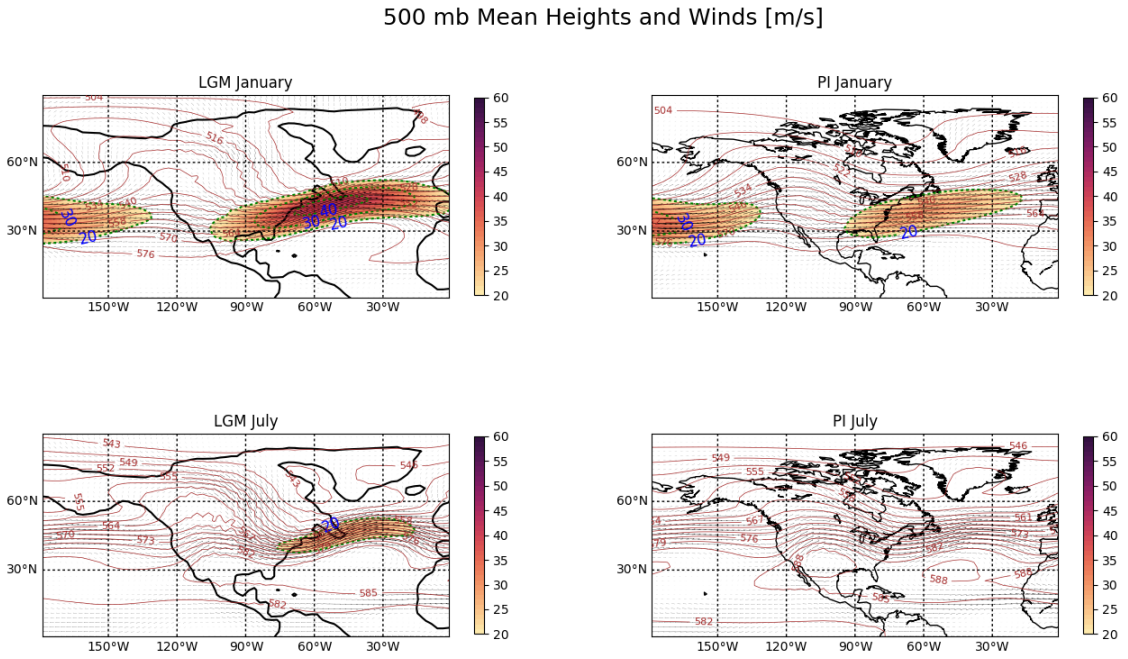

Figure 3.1.5: Mean geopotential heights at 500 mb. Heights are represented by brown contours. Shaded areas represent vector wind magnitudes of over 20 m/s. Green contours are added at every 10 m/s interval in the shaded regions.

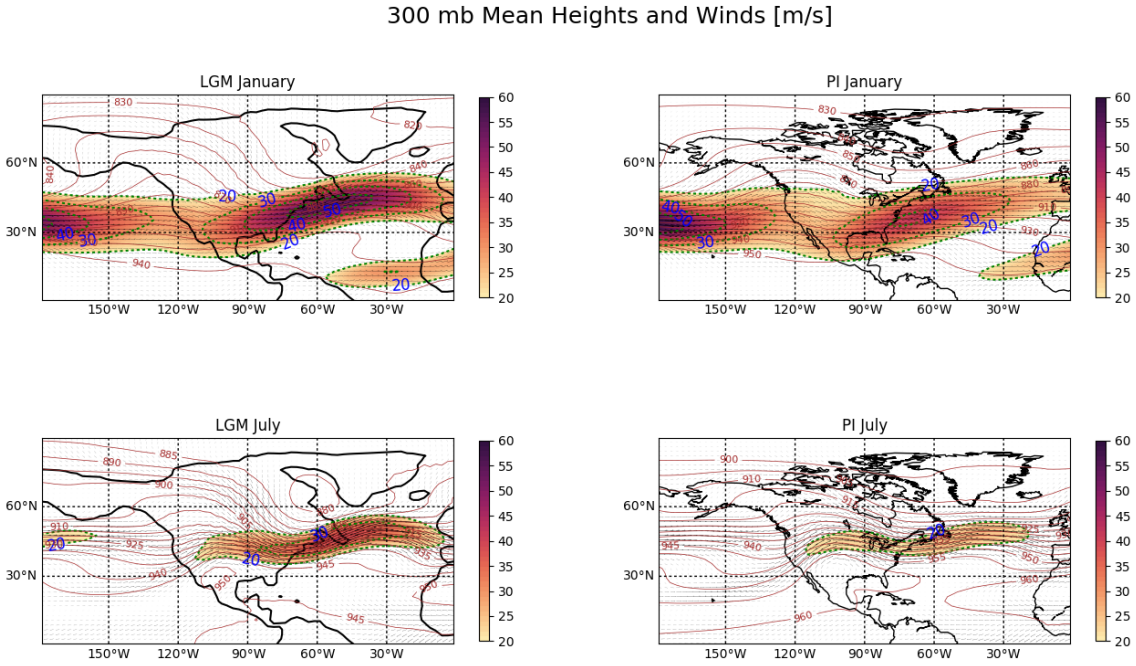

Figure 3.1.6: Includes the same features as Figure 3.5.1 but at the 300 mb level.

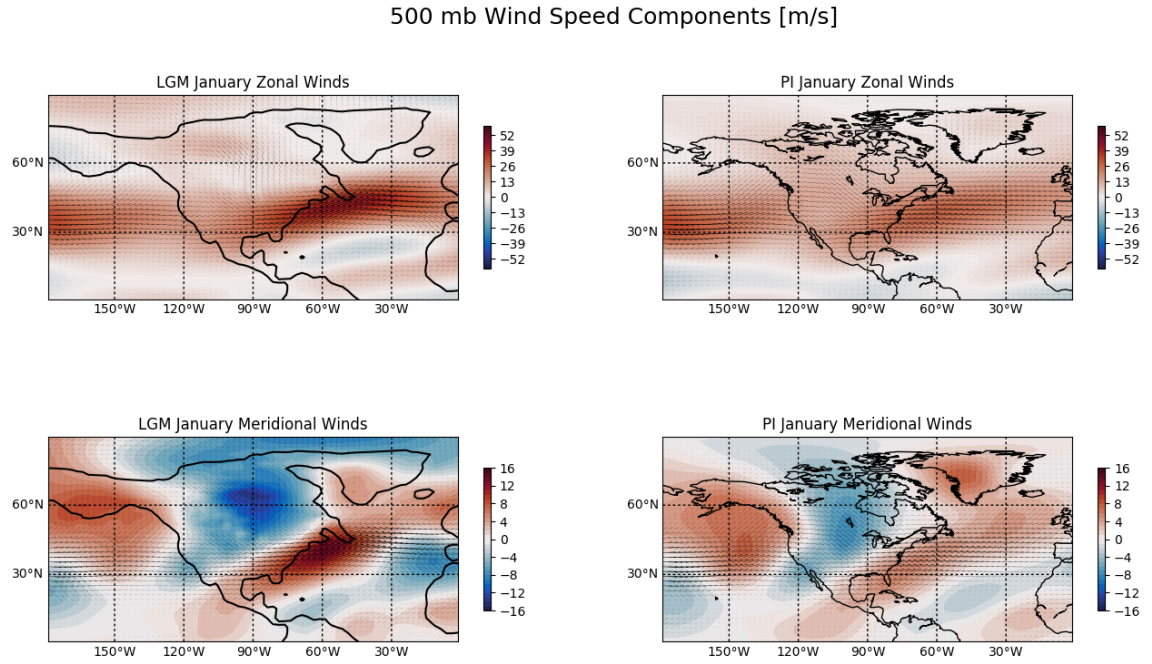

Figure 3.1.7: 500 mb wind vector components. Zonal wind speeds are shown in the top two maps. Red and blue areas represent westerly and easterly wind component direction, respectively. The bottom two maps show meridional wind speeds. Red and blue areas represent southerly and northerly wind direction, respectively.

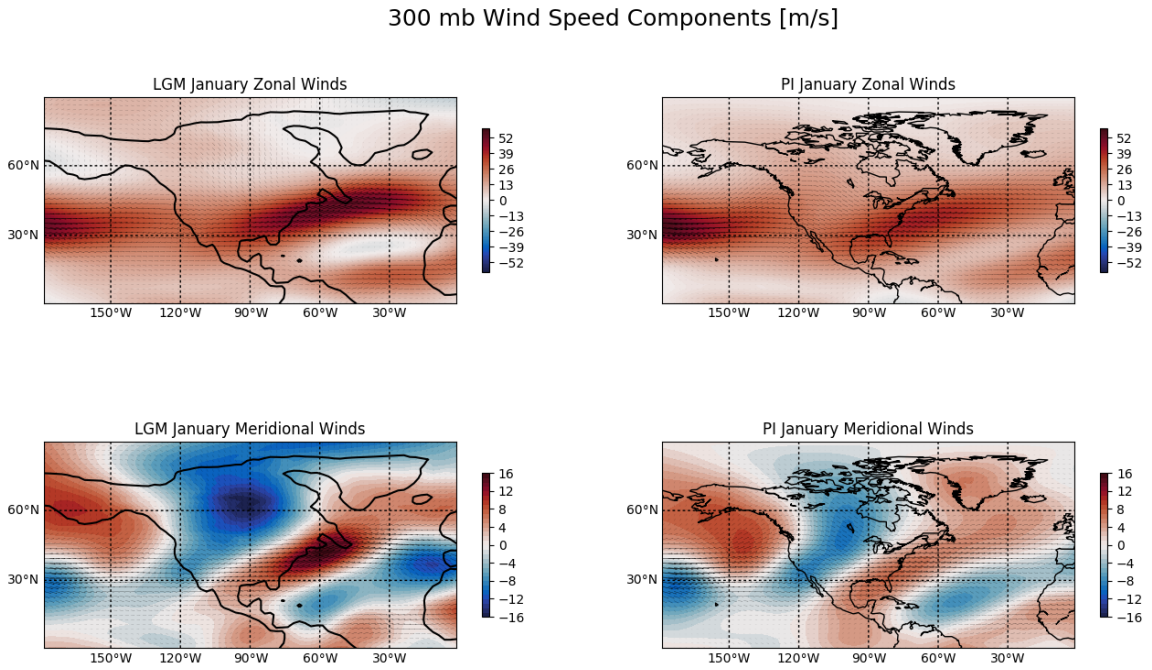

Figure 3.1.8: Includes the same features as Figure 3.5.3 at the 300 mb level.

In Figure 3.1.9, the vertical wind shear between 200 hPa and surface zonal winds have dramatic differences over ocean areas in January. The strengthened jet has the most influence on the increase of thermal wind over the Atlantic. It appears to be directly influenced by the LIS over the storm track entrance. In July, the thermal wind is increased across a zonal band over North America before shifting poleward into the Atlantic storm track. In both runs, the vertical wind shear is stronger in winter.

The thermal wind balance adjusts itself to suit the changes in topography. PI January thermal wind reflects the meridional temperature gradient created by the outflow of polar air by stationary waves induced by the Rockies along the subtropical ridge. A strong thermal wind is situated over the coasts of the Gulf of Mexico and the east coast North America which is enhanced by the Appalachian Mountains. In LGM, the thermal wind starts to recede from the Gulf of Mexico but is extended well across the east coast of North America and south of Greenland. The shape and orientation of the thermal wind mirrors that of LIS topography. There is also a local maximum to the north of the LIS maximum elevation.

As the meridional temperature gradient is eases in July, the thermal wind is weakening substantially. In PI, it is situated well within the mid-latitudes as the subtropical ridge gains strength. The thermal wind is found on the lee side of the Rockies and Appalachians. Maxima appear where cold continental winds blow over the Gulf Stream. Although the thermal wind is stronger in LGM, it is in the same position along the southern margin of the LIS.

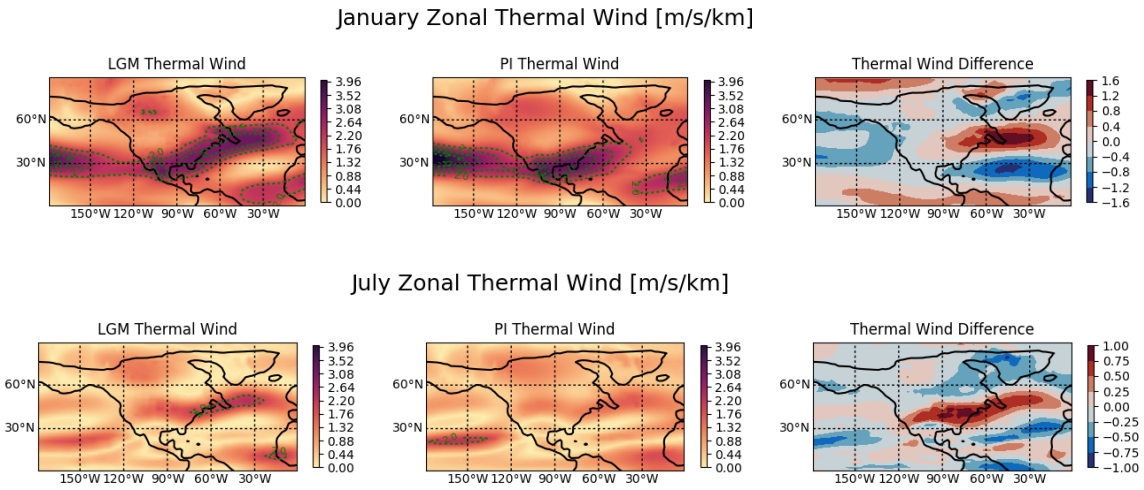

Figure 3.1.9: Zonal thermal wind between 200 hPa and the surface is depicted in the left two columns. Change of speed with height is shaded. Green contours are at intervals of 0.5 m/s/km at or above 2. The rightmost maps depict the difference with red and blue areas showing a stronger and weaker thermal wind in the LGM, respectively. Note: LGM coastlines are incorrectly imposed on PI.

In jet entrance regions, positive vertical pressure velocity or subsiding air is found to the north of the jet over a cold continental surface as depicted in Figure 3.1.10. Rising maritime tropical air is found to the south of the jet as part of a thermally direct circulation. The opposite is true for the exit region, where subsidence occurs in the subtropics and rising air in the high latitudes. In the LGM, subsidence occurs to the north of the Atlantic storm track entrance over the LIS. In the difference map, there is a stronger circulation about the jet entrance for the LGM by about 0.15 Pa/s. As for both exit regions, there are stronger circulations as well, but not to the same degree.

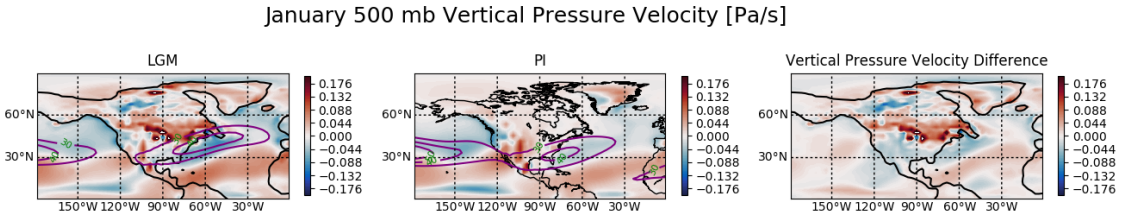

Figure 3.1.10: Vertical pressure velocities are depicted. Red and blue areas denote negative and positive pressure velocities which correspond to sinking and rising air, respectively. Purple contours outline the 30 and 40 m/s velocity wind speeds to represent the mean jet location.

3.2 BAND PASS FILTERED QUANTITIES

Standard deviation of the BPF January and July time series is used to analyze the variability in surface air temperature on synoptic time scales as shown in Figure 3.2.1. During the PI run, variability increases steadily toward the interior of the continent and toward higher latitudes. This is more pronounced in January than July as maximum values approached 4 K as opposed to 2 K. Factors such as diabatic heating, topography provided by the Rocky Mountains, jet location, and storm track entrance and exit positions allow synoptic scale eddies to propagate into the interior of the continent. The Pacific storm track exit region appear over the North Pacific as a local maximum of temperature variability. Temperature variability also increases in the western North Atlantic where the Gulf Stream lies in proximity to the cold continental surface along the east coast of North America. In July, variability over land and ocean shifts poleward. Over land it retreats farther inland, with maximum variability centered around Hudson Bay.

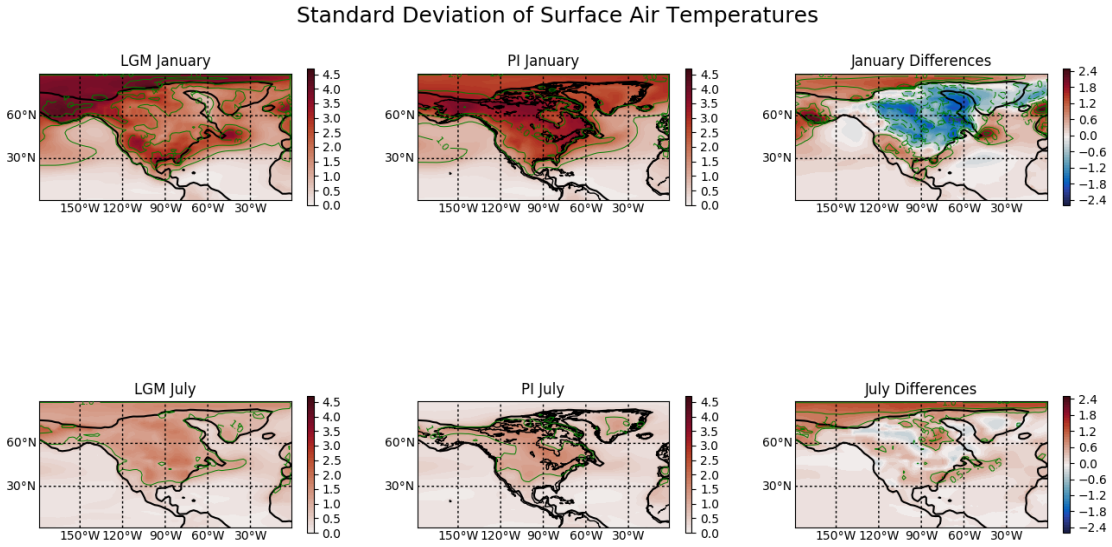

Figure 3.2.11: Standard deviation of band pass filtered surface air temperatures. Darker shading depicts higher variability of temperatures in the two leftmost columns. Contours are at interval of 1 standard deviation. Differences are calculated in the rightmost column with red and blue shading indicating higher and lower variability in LGM, respectively. Contours are at intervals of 0.5.

In the January LGM run, there is a wholesale decrease in variability over the ice sheets compared to PI due to the decrease of transient eddy activity. There are two minor decreases in variability over large ocean areas. One is in the North Pacific extending from the Pacific Northwest to the Gulf of Alaska. The other is in the subtropical North Atlantic. The Northern half experienced widespread increases up to the sea ice edges near Greenland and Iceland. Variability has pronounced increases including local maxima over the Beringia and just east of the Gulf of Saint Lawrence in the storm track entrance. There are also increases of variability just south of the ice sheet edge. The storm track entrance maxima are relatively compressed and have a tight gradient between its own maximum and strong minimum several hundred kilometers to the northwest over the LIS. This is a slight poleward shift from the comparable PI maximum that occurs despite the gradient in mean temperature shifting equatorward.

In the July run, decreased variability of the LGM nearly vanishes. The ice sheet has shown an increase of variability over the PI run over the Great Lakes, Hudson Bay, and along the entire southern margin. Increases encompass the entire North Atlantic and over the sea ice toward the southern tip of Greenland. The decrease of variability over the Eastern North Pacific remains and grew slightly larger. The difference map displays the same southwest to northwest tilted orientation of increased variability over the east coast of North America. Overall, variability is more extreme and localized during January. Values approaching and exceeding 3 K trace the margins of the LIS. Transient eddies preferentially resist propagating into the ice sheet. In July, variability is more moderate and widespread. Transient eddy activity is present over the LIS.

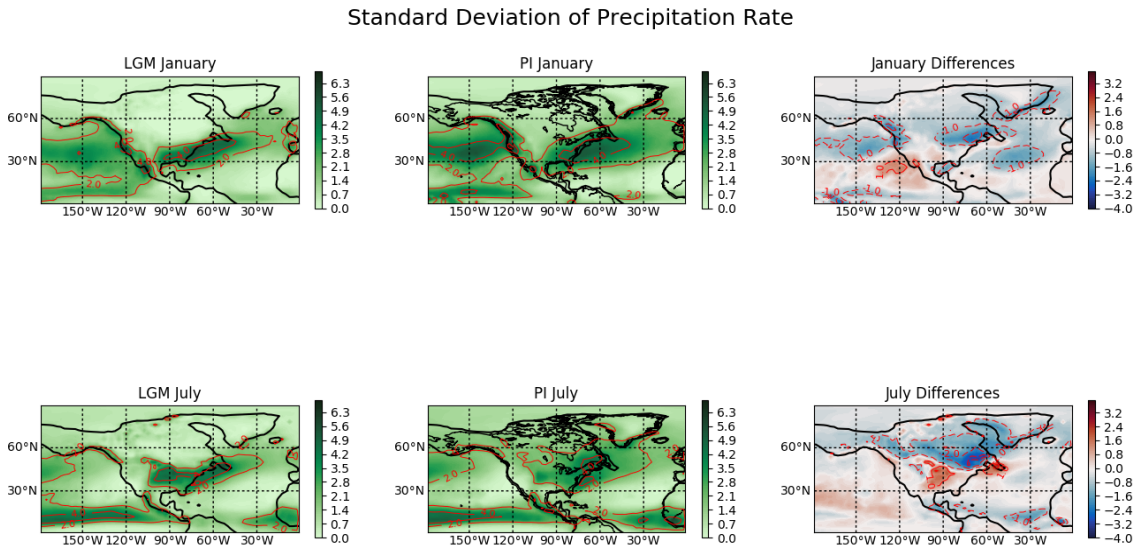

Figure 3.2.12: Standard deviations of band pass filtered daily precipitation rates. Darker shades depict higher variability of precipitation rate. Contours are at intervals of 2 standard deviations. Difference maps on the right show higher and lower variability in LGM for red and blue areas, respectively. Contours are at intervals of 1.

Despite lower water vapor content, there are some increases of BPF precipitation rate variability in LGM. Depicted in Figure 3.2.2, there is a minor increase over the southwest North

America including the adjacent ocean area for January. In July, LGM precipitation is more variable in the continental United States and Nova Scotia.

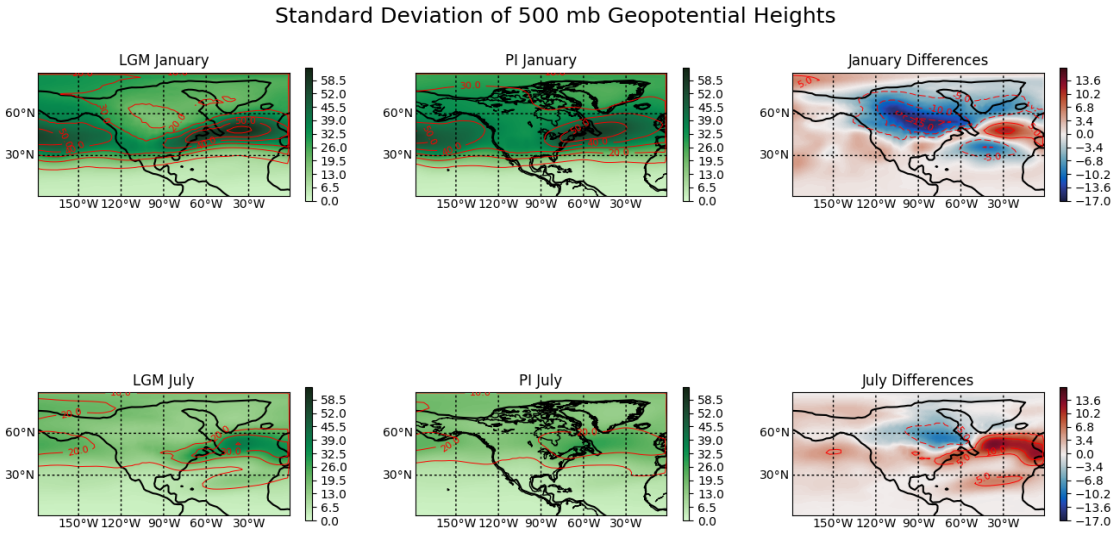

Figure 3.2.13: Standard deviation of band pass filtered 500 mb geopotential heights. Darker shading depicts higher variability. Contours intervals are at 10 m. Difference maps on the right depict higher and lower variability in LGM in red and blue areas, respectively.

Standard deviation of BPF geopotential heights are calculated at the 500 hPa level as depicted in Figure 3.2.3. The maximum of variability is centered above the North Atlantic storm track entrance and surrounded by a sharp gradient in the January PI 500 hPa run. Relative to the PI run, this area of height variability is increased and elongated along a very narrow corridor. This corridor has a southwest to northeast tilted orientation over the east coast and extending into the North Atlantic. The maximum difference is centered in the eastern portion of the Atlantic where the jet exit region resides. The variability decreases dramatically over the ice sheet and the Azores straddling this corridor. This shows transient eddy activity is particularly concentrated within this narrow corridor. Transient eddy activity also decreases in the Gulf of Alaska extending as far south as 50° N. South of there, there are increases nearly over the entire

North Pacific with local maxima along the west coast of the North American Southwest. There are also increases along the southern tier of the present day United States and the Gulf of Mexico.

In July, the decrease of variability over the ice sheets lessens with its center near the Hudson Bay. These areas extend to the sea ice margin. The only other decrease is found over the Gulf of Mexico and Central America which appears to be extending from the ITCZ. Both storm track regions appear enhanced compared to PI and in particular, the eastern portions.

The 300 hPa maps are quite similar to 500 hPa and only exceptions will be mentioned. The January LGM map display less variability across the whole region except for the North Atlantic from 45-55° N. This appears to be a reflection of increased strength of zonal flow in the upper troposphere in the LGM simulation. Maximum decreases appear above the LIS and Azores Highs.

3.3 ANALYSIS OF BAROCLINIC INSTABILITY

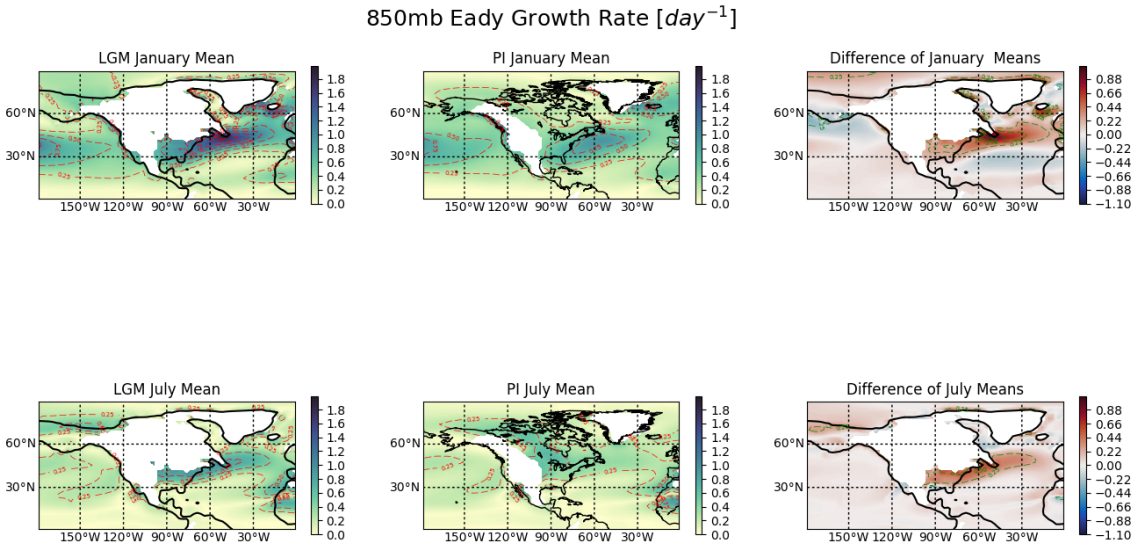

Figure 3.2.14: Monthly mean maximum Eady growth rates at the 850 mb level. The two leftmost columns depict darker shades for stronger baroclinic instability. The rightmost column is the difference between LGM and PI. Contours are at intervals of 0.25 for all maps. White areas indicate missing data due to topography reducing surface pressure below the selected pressure level.

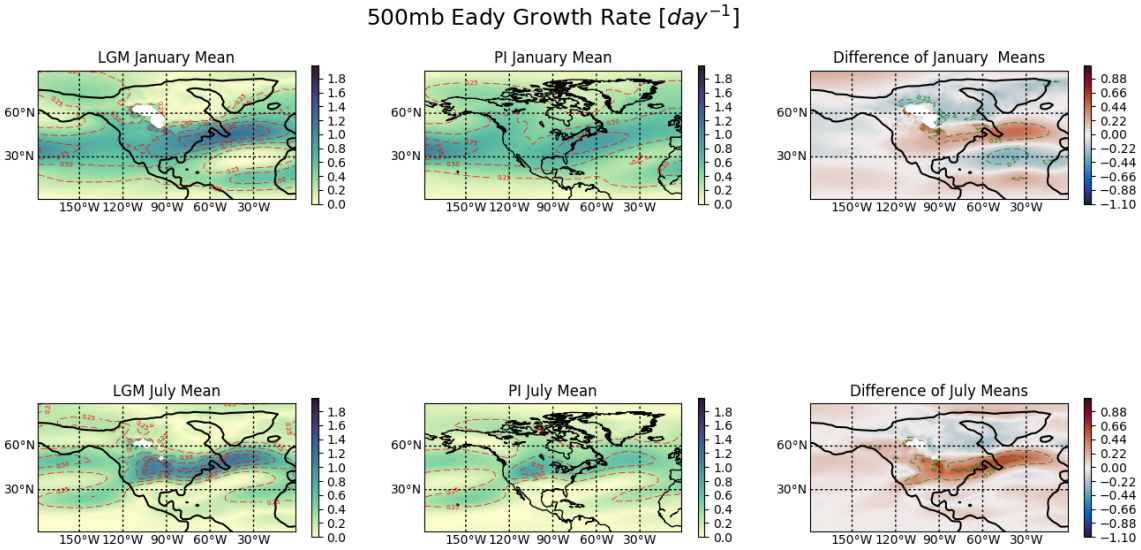

Figure 3.2.15: The same data is depicted here as in Figure 3.6.1 but for the 500 mb level.

Eady growth rate is calculated for the 850 and 500 hPa for January and July shown in Figures 3.2.4 and 3.2.5. For both levels, the LGM has more baroclinic instability extending from

the lee side of the Rockies to the entire length of the North Atlantic storm track. The poleward tilt in the entrance region is apparent for Eady growth as well. The Pacific storm track has minor increases except for January at 500 hPa. In January, the Eady growth rate has a higher maximum value compared to July but is centered off the coast of Nova Scotia, southeast of the LIS. The orientation of this area of instability is nearly zonal. July has seen more moderate values with its maximum values value located several hundred kilometers upstream. For both cases, maximum instability is located off of the southern edge of the ice sheet. The 500 hPa chart shows that baroclinic instability in the LGM is higher than the PI as far as 10-12 degrees of latitude north of the ice sheet margin. Also at 500 hPa, the LGM shows a higher increase in July compared to January. Generally, unglaciated continental areas are more baroclinically unstable. Decreases are found over the ice sheets year-round although January decreases are larger. There are also decreases in the subtropical North Atlantic and the Gulf of Alaska in January.

Eady growth rate is broken into two components for analysis of a dominant mechanism within baroclinic instability. It is dependent on vertical wind shear and static stability. The vertical wind shear term is directly proportional to baroclinic instability. Increases of the meridional temperature gradient near the ice sheet increases wind shear and therefore baroclinic instability. The static stability term is inversely proportional to Eady growth rate. Increases in static stability due to cooling of near surface temperatures in the presence of the ice sheet decreases the baroclinic instability. The presence of the LIS provides increases to both terms where static stability acts to suppress baroclinic instability and vertical wind shear enhances instability. The dominant term explains the variations and locality of Eady growth rate.

The static stability term of the Eady growth rate are analyzed at the 850 and 500 hPa levels depicted in Figures 3.2.6 and 3.2.7. Values are higher to the south of the ice sheets and along the sea ice margin at 850 hPa for both months. At 500 hPa, values are highest on the

northern side of the baroclinic instability above the ice sheet for January only. Generally, the middle and high latitudes are more stable and the tropics are less stable in January. In July, only the ice sheets have a higher stability. Other than that, there are minimal to no differences between LGM and PI.

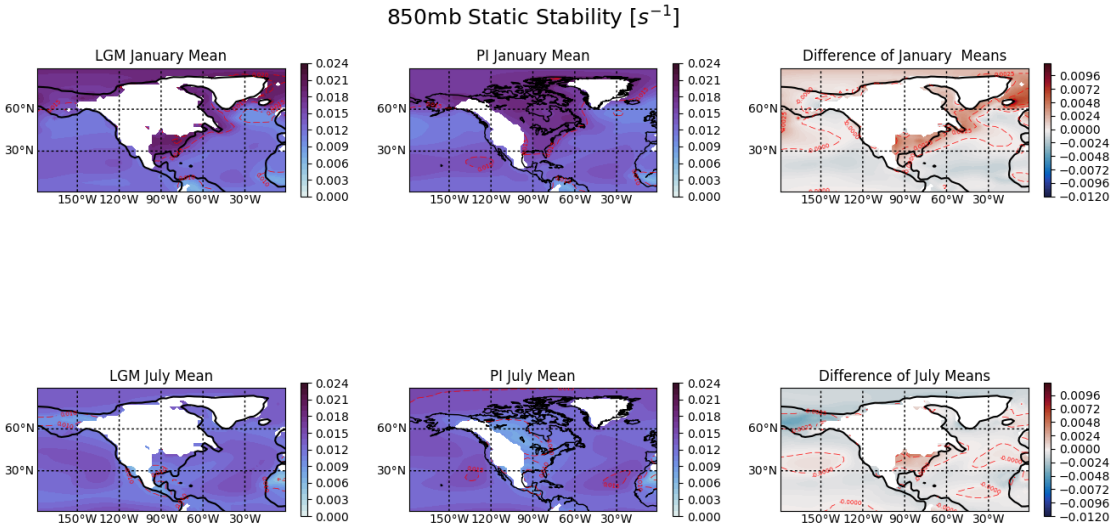

Figure 3.2.16: The static stability term of the maximum Eady growth rate at 850 mb is depicted as Brunt-Vaisala frequency N. For the two leftmost columns, darker purple area indicated a more stable atmosphere. Contours are at 0.005 intervals. The rightmost column depicts differences where red and blue indicate a more stable and unstable atmosphere in the LGM, respectively. Contours are at intervals of 0.0025.

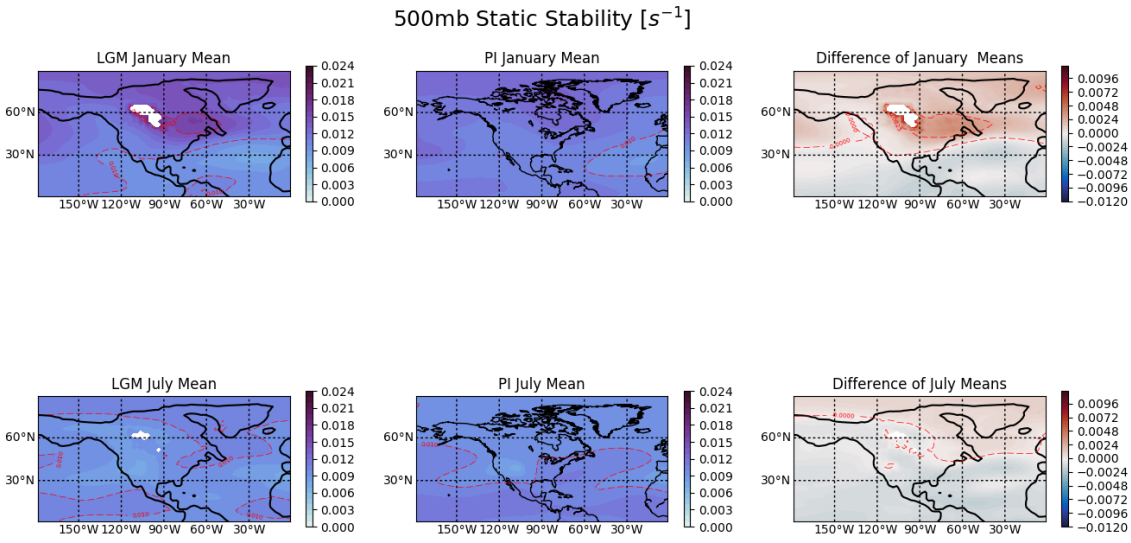

Figure 3.2.17: The same data here is depicted in Figure 3.6.3 except for the 500 mb level.

The same analysis is made for the vertical shear term depicted in Figures 3.2.8 and 3.2.9. Larger variations of wind shear relative to static stability made it the dominant term for baroclinic instability. The differences followed the same orientation and maximum value placement as with Eady growth rate. There are larger differences in January particularly at the 850 hPa level.

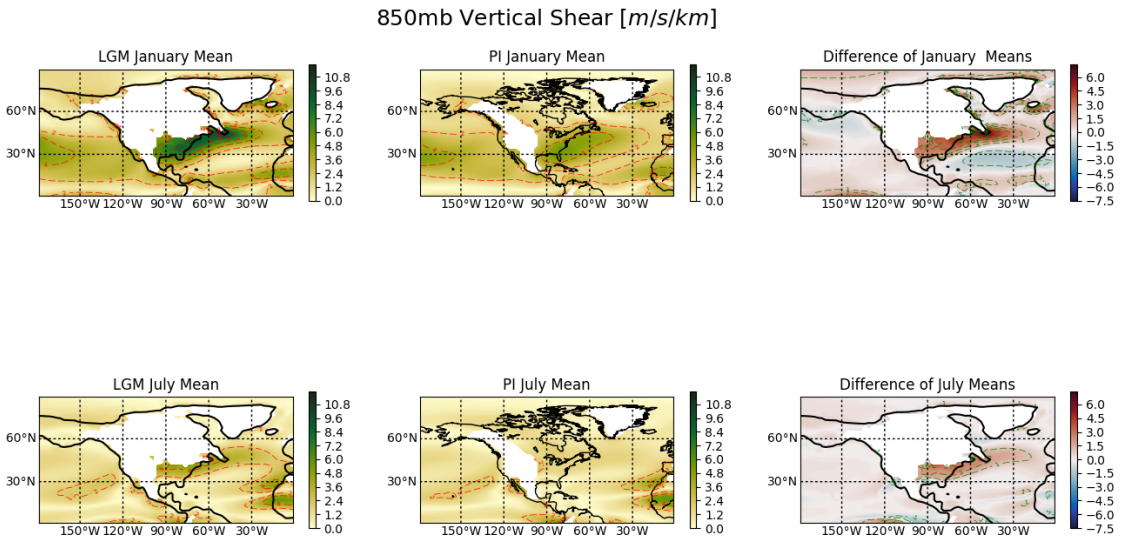

Figure 3.2.18: Depicted is the zonal geostrophic wind shear term in the maximum Eady growth rate for the 850 mb level. For the two leftmost columns, darker green shading represents stronger vertical shear with contours at intervals of 2. The rightmost column depicts differences in vertical shear where red and blue areas depict stronger and weaker shear in the LGM, respectively. Contours are at intervals of 1 above and below zero.

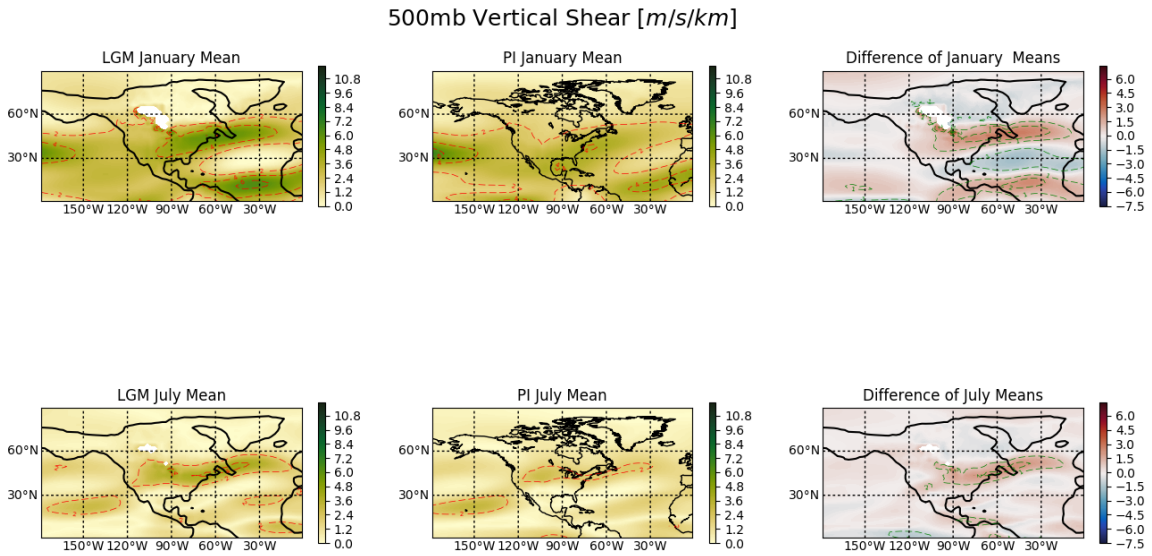

Figure 3.2.19: The same data in Figure 3.6.5 is depicted here but at the 500 mb level.

3.4 TIME SERIES ANALYSIS OF SURFACE AIR TEMPERATURES

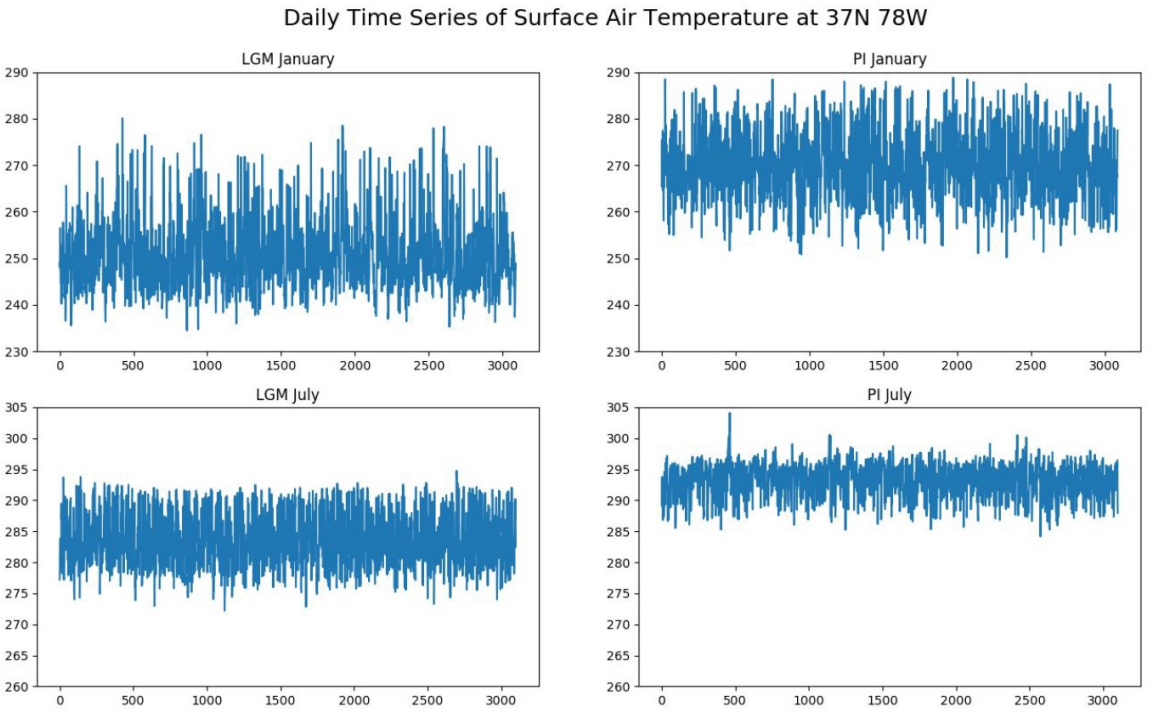

Figure 3.3.20: Time series of daily surface air temperatures for all Januarys and Julys in the 100-year LGM and PI runs. For a grid point just south of the LIS edge at 37N 78W.

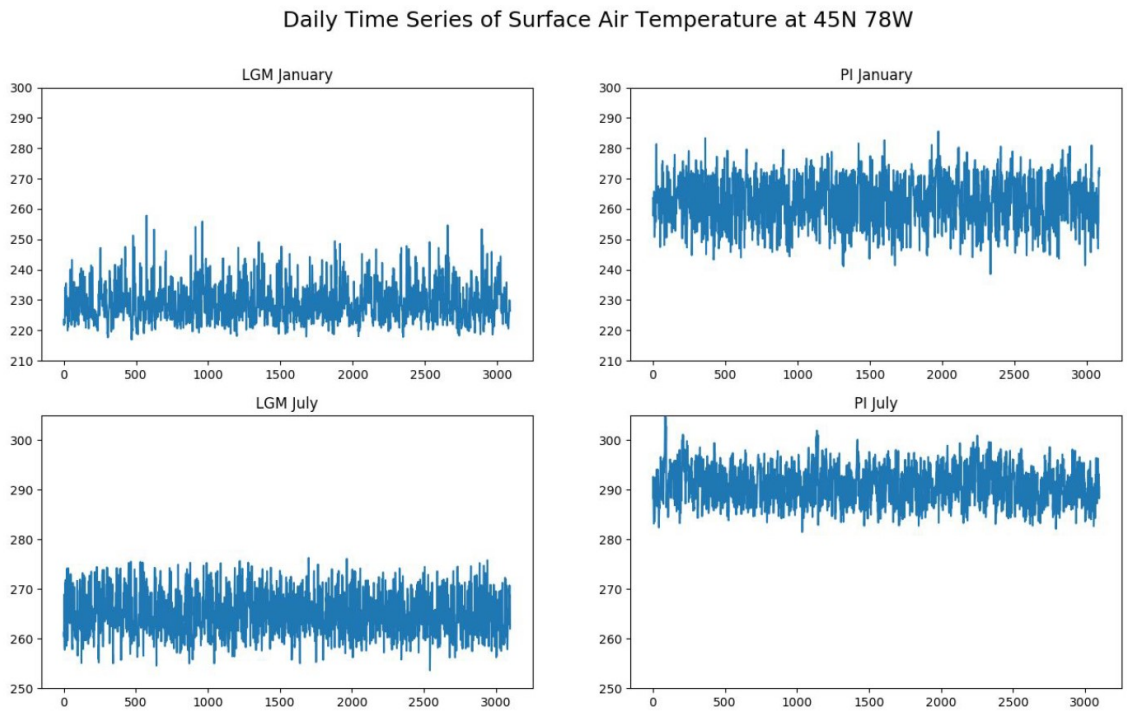

Figure 3.3.21: The same data is depicted here as in Figure 3.3.1 but at 45N 78W.

Figures 3.3.1 and 3.3.2 depict the daily surface air temperatures for all Januarys and Julys in the LGM and PI data for two selected points. Time series are produced by concatenating daily output for each respective month over the 100-year span of every simulation. These points are on the same longitude along the southeastern edge of the LIS at one model grid point north and south of the ice sheet edge. South of the LIS edge, there is a 20 K decrease of mean surface air temperature in January and a 9 K decrease in July for the LGM. North of the LIS edge, there is about a 30 K decrease of mean temperatures for both months.

The probability density functions for these time series are shown in Figure 3.3.3. Both locations at PI feature symmetric distributions indicating a relatively equal probability of positive and negative anomalies. PI July has a greater density about the mean temperature with fewer and smaller deviations. PI July at the southern location has a slight positive skew and the

greatest density about the mean temperature. Synoptic variability is suppressed here indicating transient eddies are not a key factor in this environment. Both locations at LGM have negative skews. The southern location exhibited the same peak probability at the mean value for both LGM and PI. In the LGM, there is a tendency toward positive anomalies and higher extreme values for such anomalies as well. Transient eddies are not more prevalent in this case but have a larger role in heat transport in the LGM. The southern location has a slightly larger range of variability in LGM compared to PI. In LGM July, there is almost a bimodal distribution that shows an increased frequency of positive anomalies. The probability of mean temperature is close to 9% as opposed to 16% in PI. Transient eddy activity has increased here in July where it had not changed much in January.

In the northern location, there is a large distribution of temperatures about the mean indicating suppression of transient eddy activity over the LIS. There are episodes of large extremes toward warming in January. Transient eddies are not as prevalent here but had a greater role of heat transport since northerly flow dominated. Although significantly cooler in July, this ice sheet location resembles the distribution of temperatures in PI. Transient eddy activity at this location in July is slightly higher in July.

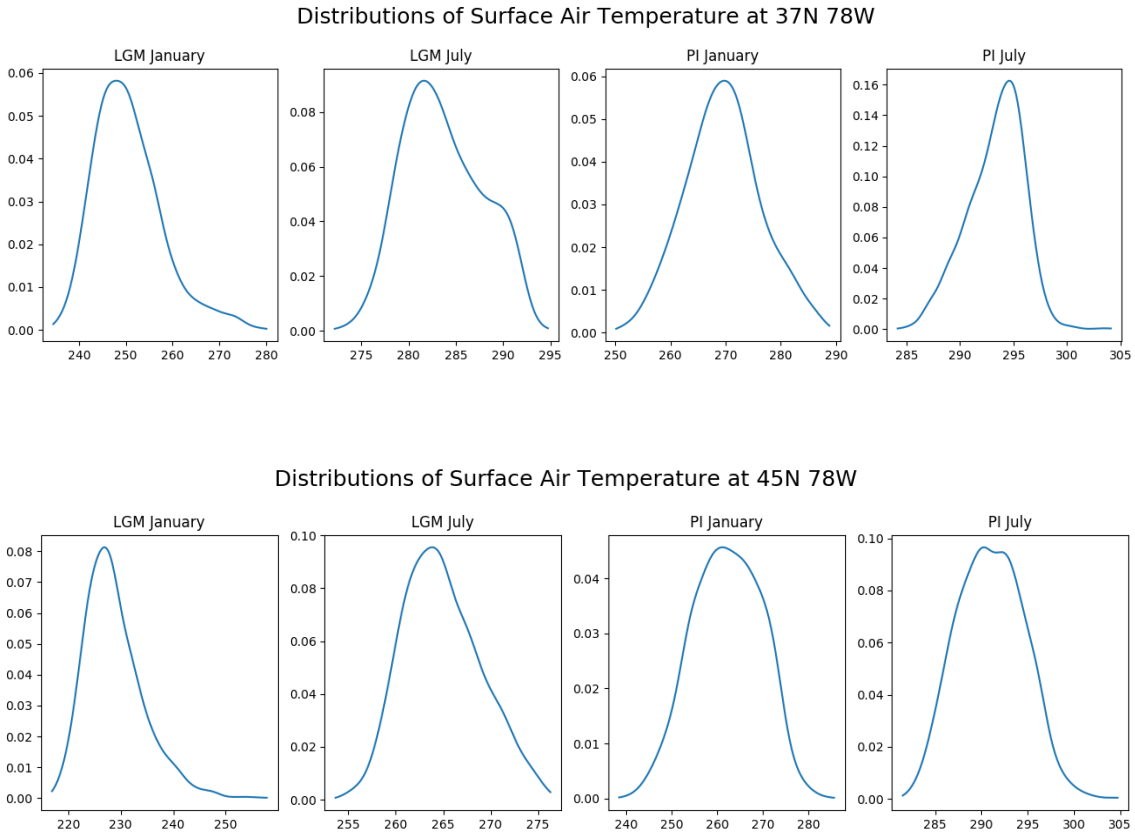

Figure 3.22: Probability density functions of the daily time series of surface air temperatures for the two selected points. Temperature is shown on the x-axis in units of K. The probability is depicted on the y-axis.

3.5 ANIMATIONS

Animations are created using daily SLP, precipitation, and 2-m reference temperature. These three variable outputs are averages over the entire day. These animation files are stored as supplementary files with the thesis pdf in the RUCore repository and made available for public view. In LGM January, unstable waves form in the baroclinic zone near the Gulf of Mexico and are typically seeded by Pacific cyclones that remain with the southerly mean flow. These transient eddies do not migrate poleward of the Pacific Northwest and bring precipitation to the North American Southwest. Although eddies underwent barotropic conversion approaching the Pacific jet exit region, there is enough baroclinic structure within the transient eddies to remain as disturbances in the atmosphere. As they traverse the North American continent, these disturbances are susceptible to unstable growth. Most of the precipitation is offshore of the east coast, however there are episodes of precipitation along the southern edge of the ice sheet and north of the Gulf of Mexico. Since it is usually well within the freezing line, it is assumed to be snowfall which would have added ice mass to the ice sheet in an attempt to maintain or grow the LIS.

Pacific cyclones that migrate north of the Pacific Northwest are swept into the upper level block created by the LIS. These cyclones follow the coast of North America along the Gulf of Alaska before entering Beringia. Other cyclones simply migrate straight northward through Beringia or to its west. The result is the same, they enter deep within the Arctic Circle and either dissipate or migrate along the northern edge of the LIS and appear near Greenland. In January, there are almost no eddies that migrate into the LIS.

Cyclones grow rapidly within the North Atlantic storm track entrance and are usually fed by unstable waves originating from the Gulf of Mexico or the lee side of the Appalachians.

Precipitation values decrease sharply as eddies traverse offshore of 45° N. Typically, cyclones migrate toward western Europe and face barotropic conversion by the western continental ridge. The dissipating cyclones migrate north along the European coast before either circulating back toward Greenland adding snowfall to the sea ice of GIS or migrating northeast toward the Norwegian Sea. Other eddies migrate poleward sooner and head straight to Greenland or Iceland. Cyclones do not appear as mature as their PI counterparts and tend to be more zonally elongated. Since model output variables are daily averages, then faster propagation of transient eddies may create more zonal elongation in the output. Less mature eddy structures may also contribute to the zonal elongation. Separating these contributions is not something that is explored in the thesis.

In PI January, unstable waves also form near the Gulf of Mexico but also further north along the lee side of the Rockies. Pacific cyclones typically migrate through western North America feeding directly into the North Atlantic storm track. Cyclones that enter Alaska typically traverse northern Canada as dissipating disturbances. Hydrological feedbacks occur with these baroclinic waves as they near the east coast. Cyclones are distributed more evenly poleward of the North Atlantic storm track. They typically follow simpler trajectories toward the northeast compared to LGM. Equatorward tilting of upper level flow in the LGM eastern Atlantic is present to inhibit poleward migration of transient eddies that remain with the track. Disturbances that fed the storm track tend to start the maturation process before entering the storm track. The eddies tend to be more meridionally elongated over the Atlantic compared to the LGM cyclones.

In July, a weakened LIS High and strengthened North Pacific High allow Pacific cyclones to traverse North America along the southern margin of the LIS. They usually enter the Pacific Northwest. These baroclinic waves still face dissipation from barotropic regimes but they feed directly into the baroclinic zone on the lee side of the Rockies. There are notable increases of

precipitation in the Midwest where there is a sudden northerly retreat of the LIS. Similar to PI, the subtropical ridge dominates the Gulf of Mexico preventing baroclinic waves from developing there. Lee side effects from the Appalachians allow transient eddies to develop along the east coast. Unlike January, Pacific cyclones migrate across all latitudes over the LIS. BPF variability of temperature, precipitation, and heights over the LIS, although low, is relatively uniform and not prohibitive.

Pacific cyclones are able to travel along the LIS margin and seed disturbances into the Atlantic storm track. The barotropic shear over western Europe lessens compared to January allowing more cyclones to follow straighter, poleward paths. Compared to PI July, there is more synoptic variability over the Atlantic with the exception of high elevations in Greenland and precipitation due to a dampened hydrological cycle. However, it seems the North Atlantic storm track entrance is the most active region for variability. The LIS has the most direct effect on the storm track changes considering the thermal wind and temperature gradient. Temperature variability in the eastern Atlantic is similar to PI.

In PI July, Pacific cyclones do not typically reach landfall south of Alberta. It is the weakest regime concerning baroclinic instability with a small maximum north of Colorado. Unstable waves typically migrate through Canada or develop off the east coast.

4 DISCUSSION

Lau (1978) finds a decelerated mean flow along with super-geostrophic winds in the jet exit region of the Eastern North Pacific indicating a strong ridge. Eddy kinetic energy is converted to potential energy as the flow becomes barotropic. This is consistent with the PI run. LIS topography has a noticeable effect on the LGM mean flow of the eastern Pacific and the termination of the North Pacific storm track. The 500 hPa and 300 hPa mean height charts depict the enhanced ridging situation in the high latitudes as described in Manabe and Broccoli (1985). A lowered tropopause and increase of surface elevations divert the mean flow to the north to conserve potential vorticity. This effect is stronger during winter due to a colder troposphere and strengthened westerlies. Westerlies decelerate and become more southerly.

Blocking induced by the LIS High shows a split flow which included the enhanced mid-high tropospheric ridge in the high latitudes as explained earlier as well as a zonal structure in the mid latitudes similar to PI. The mean jet is similar to PI as well however there is more of an equatorward tilt as jet approached the continent. LGM enhanced barotropic shear of the jet (Donohue and Battisti, 2009) has implications on eddy structure that reduces dynamic tilting and eddy heat transport. Energy that is lost when storms enter anticyclonic rotation is absorbed into the zonal mean flow. Justino et al. (2005) attribute momentum flux convergences by stationary waves to weaken the zonal mean jet. They find that transient eddies propagate slower and their structures are more zonally elongated in 500 hPa decelerated Westerlies.

Transient eddies that exit the North Pacific and dissipate into the mean flow over North America as baroclinic disturbances alter synoptic variability over the continent with respect to changes in the mean flow. Transient eddy activity over North America is dependent on the seeding of North Pacific cyclones. Propagation of these eddies entering the region is not only

directed by mean flow steering but by their initial entry points into the mean flow. Upstream changes of propagation are determined by alterations to the North Pacific storm track.

The North Pacific storm track is defined by the analysis of BPF 500 hPa geopotential heights. The BPF isolate the synoptic time scale and measures the variability of heights by synoptic disturbances (Blackmon, 1976). The frequency of the temporal filter excludes contributions by planetary scale waves and diurnal variations. In the North Pacific, the variability of these heights has been elongated on its eastern portion and shifts to the south. Laine et al. (2008) demonstrates an identical structure with the storm track. What is interesting is the strong reduction of variability approaching the LIS.

In January, variability of geopotential heights is restricted to the coasts with extensions toward Beringia, the Pacific Northwest, and the North American Southwest. Variability of surface air temperatures suggest the bulk of these synoptic eddies are concentrated to the north over Beringia while there are some occurrences toward the Pacific Northwest and North American Southwest. Poleward transport of heat by transient eddies is responsible for the inhibition of ice sheet growth in Alaska. Bromwich et al (2004) observes cyclone tracks using 6-hour mean SLP values. The majority of these tracks are across Beringia where cyclones eventually dissipate over Arctic sea ice to the North of the continent. A minority of cyclone tracks is also observed heading into the Pacific Northwest or to its south.

Unterman et al. (2011) attribute the poleward shift of synoptic disturbances due to increased cyclogenesis in the North Pacific and mechanical forcing by the LIS. Enhanced ridging of upper level geopotential heights correlates with this. The weakened North Pacific High permits more cyclones to remain in the south if they did not follow the strong poleward tendency of the track. A small concentration of these eddies migrates toward the North American Southwest which is consistent with Oster et al. (2015).

As these cyclones leave the jet exit region, they enter their dissipation stages. Cyclones that move into Beringia do not bring significant precipitation inland as it is far from the mean flow and the circulation of the Aleutian low return toward the Pacific. Precipitation is transported further inland by cyclones that migrate equatorward due to the strengthened mean flow. Oster et al. (2015) note this as well for storms entering the Pacific Northwest or to the south as steered by a strengthened, zonalized jet entering North America.

In July, the Pacific storm track shifts poleward with its exit region in the Gulf of Alaska. The blocking situation aloft is relaxed allowing for a more zonal flow into the northwest of the continent which is consistent with Bromwich et al. (2004). They also observe cyclone tracks shifting to the south of Beringia and are permitted to propagate into the west coast of North America. Static stability within the LIS High decreases along with reduced surface cooling. The North Pacific High also migrates west aiding this flow. The jet weakens but shifts poleward leading into the region. Synoptic eddies traverse into the LIS and continue to enter Beringia but there is precipitation further inland. BPF surface air temperatures are rather uniform poleward of 40° N on the western continent.

LIS topography has a significant impact on the geopotential height field. Equatorward of 40° N, mean flow in January closely resembles that of PI. The flow has split north of this as a broad ridge in the west and a deep trough in the east. Zonal mean flow starts to accelerate lower in the troposphere farther west. Maximum speeds approach the North Atlantic storm track entrance in the east. The orientation of these features is also different from the PI counterparts with the ridge axis tilted to the northwest and the trough axis with a sharp tilt to the northeast. This is consistent with Manabe and Broccoli (1984). These features feed into the zonal mean flow that is compressed along the southern margin of the LIS. There is a strong northerly component of mid-upper tropospheric winds over the LIS. However, there is a sharp

transition to a strong southerly component along the East coast. In July, these features are weakened but are greater than in PI as in Bromwich et al. (2004).

The maximum elevation of the model LIS is in western Canada on the lee side of the Rockies and is mostly perpendicular to the zonal flow there. However, local maxima of LIS elevation are situated parallel to zonal flow along between 50° N – 60° N. The northern extent of the zonal mean jet is adjacent to the local elevation maxima. Rossby waves induced by this topography has a very sharp tilt to the northeast as a result. The merging of upper level flow accelerates the jet giving it a poleward tilt along the east coast of North America.

The LIS High is established due to massive surface cooling related to albedo decreases and elevation increases (Gates, 1976). The barotropic structure is at maximum strength in January and provides anticyclonic circulation which dominates the environment of North America. Northerly surface winds flow down the decline of elevation along the southern margin of the sheet providing polar air over the unglaciated landmass north of the Gulf of Mexico. Surface zonal flow is suppressed, and the heat capacity of the Gulf allows mixing of subtropical air to occur. In July, increased diabatic heating is controlled by southwesterly flow from the North American Southwest. This is strongest in the Midwest United States compared to the southeastern coast which explain the lack of ice mass there and the shape of the LIS.

The thermal wind is representative of areas of high baroclinicity. The increase of barotropic energy over the LIS (Justino et al., 2005) suggests there is higher baroclinicity to shed this energy by cyclogenesis (Cai and Mak, 1990). Branstator (1995) finds that the barotropic component of planetary scale affects the steering of baroclinic waves and perturbations to the large-scale waves acts to reorganize oceanic storm tracks. Maximum Eady growth rate suggests a highly baroclinic environment along the southern margin of the ice sheet to the south and especially on the lee side of the Rockies. In July, baroclinicity recedes away from the Gulf of

Mexico. Although static stability increases in the LGM which would suppress baroclinicity, the increases of vertical wind shear as shown in the results section dominates changes to baroclinicity. Since the topography and temperature gradient enhances the thermal wind, would it suggest that the thermal wind balance is integral to controlling the shape and extent of the ice sheet?

Transient eddy activity over North America has different patterns between January and July in the LGM run. BPF variability and animations display the aversion of transient eddies to the LIS in January. The Rocky Mountains also disrupts the propagation of Pacific cyclones into North America. However, BPF temperature and precipitation show increased transport on the synoptic time scale in the North American Southwest. Oster et al., (2015) suggests this mechanism for increased precipitation in the region which maintains pluvial lakes. Model output variables do not include horizontal heat fluxes so further investigation into transient eddy heat transport over continental North America is not explored. The literature has described the role of transient eddies with respect to heat transport over ocean areas in the storm tracks for the LGM quite thoroughly (Justino et al., 2005; Li and Battisti, 2008; Laine et al., 2008; Donohue and Battisti, 2009). Reductions in sensible and latent heating due to decreases in average global temperatures and atmospheric water vapor poses an interesting question in how transient eddies transport heat over North America and should be investigated. This is further exacerbated by Pacific cyclones being diverted north toward Beringia where eddy heat fluxes do not feed into the interior of the continent. In this case, oceanic storm tracks serve to reduce the equator to pole heat differential and deprives North America of heat transports by migratory cyclones. Does this mechanism aid in promoting LIS growth during January?

Transient eddies reform on the lee side of the Rockies for baroclinic disturbances that did propagate into the continent. Most of these eddies reform along the thermal wind balance

established over the Gulf of Mexico coastline. These transient eddies provide little to no increase of BPF temperature and precipitation to the south of the LIS as compared to PI values. Yet BPF geopotential heights and Eady growth rate suggests that there should have been increased transient eddy activity due to the increase of baroclinicity. Diversion of North Pacific cyclones seen in the animations and correlate with the literature (Donohue and Battisti 2009; Unterman et al., 2011) suggesting that areas with high baroclinicity need to be seeded properly. Donohue and Battisti (2009) also finds that North Atlantic cyclones are 30% less efficient with eddy heat transport due to the deficit of North Pacific storms feeding the North Atlantic storm. These eddies do not mature fully and lack elongation of their meridional and vertical structures. Calculating new variables to measure eddy kinetic energy, momentum flux convergences, and structural properties of transient eddies would be interesting to note their role on the unglaciated continental area and on the inhibition or growth of the LIS. Model output variables do not have the components required to calculate the variables mentioned above.

In January, animations reveal most transient eddies are developing offshore in the Gulf of Mexico and the east coast. However, BPF temperature and precipitation has little to no difference compared to PI. Transient eddies, although less frequent, appear to provide an appreciable amount of heat and moisture transport over the unglaciated land mass. Time series data of the location south of the ice sheet depict similar results.

Bromwich et al., (2004) states how the weakened circulation of the LIS high permits more Pacific cyclones to migrate over the LIS. Increased surface heating reduces the subsidence of the LIS high. In PI, transient eddy activity is not prevalent south of 40° N in terms of BPF variability and Eady growth rate. For the LGM, these variables increase south of 50° N. Transient eddy activity is a key player in atmospheric dynamics in the summer time. Intrusions of transient eddies over the LIS and even the Greenland Ice Sheet would have had significant impacts of heat

and moisture fluxes for the ice sheets. Most of these eddies propagate along the ice sheet margin. 2-m reference temperature isotherms around the ice sheet edge are above freezing suggesting that transient eddies are promoting LIS melting. It would be worth investing how transient eddy activity reduce LIS ice mass. Measuring eddy heat transport is a logical next step. It would also help to quantify feedbacks that would promote or inhibit LIS melting in summer such as radiative fluxes from cloud cover, formation of meltwater pools on the ice sheet surface, strengthened southerly surface winds, and deposition of aerosols.

Another interesting study would be to measure transient eddy activity for the rest of the year. If the mechanism of eddy heat and moisture transport could be quantified year-round, then there could be a determination on the role of continental transient eddies on long term growth or inhibition of the LIS.

The southeastern margin of the LIS and southern edge of the Greenland Ice Sheet has transient eddy activity based on the contributions of the North Atlantic storm track. As mentioned in the introduction and evidenced in the results, the narrow corridor of baroclinicity leads into this storm track entrance. As with North America, the increase of baroclinicity and BPF variability becomes a more dominant feature in July. The PI temperature gradient disappears but it remains for the LGM. The interface between the LIS and Gulf Stream provides a sharp temperature contrast all year long. Thermal wind balance follows the jet and is imposed over the meridional temperature gradient. The poleward side of the jet outlines the sea ice margin. In the animations, transient eddies rapidly develop in the corridor and is more efficiently seeded by the North Pacific storm track as opposed to January. Transient eddy activity grazes the margins of the ice sheets and sea ice.

It is interesting to note that the climate just south of the ice sheet is one that is not seen in the present-day world. There is an ice sheet that terminates in the mid latitudes in a

continental interior. A simple tundra climate is hard to imagine considering the enhanced synoptic variability over this area especially during the summer. Modeling vegetation and ecosystems may exhibit some interesting findings in such a climate.

Transient eddy activity in the thesis helps to quantify the prevalence of transient eddies. What is not well understood is the frequency and intensity of these storms. Although the animations present a degree of cursory analysis, they do not give a strictly quantifiable dimension to the findings. There is need storm tracking software that can account for individual transient eddies. Measuring their individual tracks, length of period, precipitation accumulation, and changes to location temperature and pressure is valuable to understanding the effects of transient eddies in LGM simulations. It will also provide an answer for frequency and intensity.

The changes to baroclinic instability brings up the question of severe weather. The Midwest United States is notorious for severe thunderstorms and tornadoes during the spring. Eady growth rate increases in the area in July along with an increase in vertical wind shear and decrease of 500 hPa static stability. It is reasonable to suggest that severe weather in this area would become worse and merits a follow up study.

The ice sheet reconstruction used in these model runs have some important considerations in context to these analyses. The maximum elevation of the LIS is in the northwestern portion of the continent in what is now western Canada on the lee side of the Rockies. It is mostly perpendicular to the zonal flow there. However, local maxima of LIS elevation are situated parallel to zonal flow along between 50° N – 60° N. The ice sheet reconstruction used in the model is PMIP2 is based on an earlier version of Peltier's ice sheet reconstructions, ICE-5G. Thus, it is consistent with some of the literature from the previous decade (Li and Battisti, 2008; Donohue and Battisti, 2009; Laine et al., 2008; Oster et al., 2015). PMIP3 is the most recent version which is based on a composite of ice sheet reconstructions

including ICE-6G (Abe-Ouchi et al., 2015). The ICE-5G ice sheet include significantly higher elevations than ICE-4G, used in PMIP1, and ICE-6G. It also includes a well pronounced ice dome over the Western LIS absent from other versions. The ICE-6G ice sheet includes a gradual slope along the southern LIS margin and does not exhibit the "fjord-like" features in previous versions which is present in this study. Only the most recent literature (Oster et al., 2015; Lofverstrom et al., 2016) included the ICE-6G ice sheet. Other relatively recent studies still uses ICE-4G reconstruction (Bromwich et al., 2004; Justino et al., 2005; Unterman et al., 2011). These differences are important to distinguish due to the influence of topography on the storm track.

It is also important to speculate how this experiment would be different if run on the more recent ICE-6G reconstruction which is typically run on a CMIP5 climate model. Lower elevations of the ice sheet reduce the impact of topography on the thermal wind balance and therefore the baroclinicity to the south of the LIS. This would suggest a reduction of transient eddy activity relative to the model used in this thesis. Mean flow of the mid-upper troposphere would not have seen as much enhancement to the ridging along the western portion of North America and the consequent trough along the eastern portion. Interestingly though, Lofverstrom et al., (2016) models variations of LIS maximum elevations from 3000 m – 4500 m and finds that as LIS maximum elevation increases, the more zonal the polar jet becomes. One could speculate that a more zonal orientation of the mean flow would allow North Pacific cyclones to migrate into North America more effectively in January and zones of baroclinic instability. Considering the impact of improper seeding of the storm tracks in the results, this would depict an LGM with higher transient eddy activity in the North American winter. In July, the LGM may have a small shift toward resembling something closer to PI. Another study using ICE-6G (Oster et al., 2015) has the inclusion of pluvial lakes in the North American Southwest. This hydrological source region would have latent heating feedbacks on transient eddies as well

as moisture transport across the lower half of the continent. This would support the transient eddies role of inducing ice sheet melt in the summer.

Another interesting study is to compare the mechanical and thermal contributions of the ice sheet. This can be done by simulating the LIS with LIS albedo and PI topography to measure the thermal contribution. Using LIS topography and PI albedo will simulate the mechanical effects. This should clarify which is the dominant contributor to the notable thermal wind found in LGM.

5 CONCLUSIONS

Synoptic variability is simulated at the last glacial maximum in comparison to a pre-industrial control run over North America. A temporal filter is applied to variables such as temperature, precipitation, geopotential heights, and sea level pressure to isolate contributions by transient eddies on the synoptic time scale. Transient eddy activity is determined by BPF variability and maximum Eady growth rate. Variability is calculated for January and July since transient eddy activity is found to be at two extremes during those two months.

Transient eddy activity in the LGM during January is characterized by LIS suppression by massive subsidence of the LIS high. Transient eddies are diverted away from the LIS as they exited the North Pacific storm track. Transient eddies that propagate toward the LIS are swept into southerly mean flow. Most transient eddies are diverted to the north, transporting heat and moisture toward Beringia and the Arctic sea ice beyond it. The rest of the transient eddies propagate toward the Pacific Northwest or to its south. Transient eddy activity for the rest of the continent is characterized by thermal wind balance established along the coastlines of the unglaciated land mass on the lee side of mountain chains and the LIS on the east coast. Although highly baroclinic, transient eddy activity is mainly constrained offshore and eddies typically form along the Gulf of Mexico coastline. The absence of North Pacific cyclones diminishes the prevalence of transient eddies on the eastern portion of the continent including the North Atlantic storm track.

Transient eddy activity reaches its maximum over continental North America in July. A weakened LIS high and stronger zonal mean flow allows transient eddies to propagate over the LIS. The majority of transient eddy activity and BPF variability occurs along the southern margins of the LIS south of 50° N. Although all BPF variables show a low prevalence of transient

eddies for the rest of the LIS, they are homogenous in their distribution. North Pacific cyclones feed into the highly baroclinic structure produced by topography and the meridional temperature gradient. Development of transient eddies along the Gulf of Mexico coastline diminishes in favor of the east coast and to a smaller degree, the lee side of the Rockies.

Although baroclinicity in the LGM has a maximum in January, this maximum is located in the North Atlantic storm track which is dominated by vertical wind shear induced by LIS topography and the ocean-land interface. Over the unglaciated landmass, synoptic variability changes little from the PI counterpart although the spatial and temporal distribution of transient eddies has been altered. The increase of continental transient activity relative to PI is at its largest in July. The baroclinic structure over the continent is stronger and has better seeding of baroclinic disturbances. As such, increases of synoptic variability relative to PI are larger in July.

6 REFERENCES

Abe-Ouchi, A., Saito, F., Kageyama, M., Braconnot, P., Harrison, S. P., Lambeck, K., Otto-Bliesner, B. L., Peltier, W. R., Tarasov, L., Peterschmitt, J.-Y., Takahashi, K. 2015: Ice-sheet configuration in the CMIP5/PMIP3 Last Glacial Maximum experiments, *Geosci. Model Dev.,* **8**, 3621–3637

Berger, A., 1988: Milankovitch theory and climate, *Reviews of Geophysics*, **26**, 4, 624-657

Blackmon, M. L., 1976: A climatological spectral study of the 500 mb geopotential height of the Northern Hemisphere, *J. Atmos. Sci.,* **33**, 1607-1623

Blackmon, M. L., Lau, N. C., 1980: Regional characteristics of the Northern Hemisphere wintertime circulation: A comparison of the simulation of a GFDL general circulation model with observations, *J. Atmos. Sci.*, **37**, 497-513

Branstator, G., 1995: Organization of storm track anomalies by recurring low frequency circulation anomalies, *J. Atmos. Sci*., **52**, 207–226.

Bromwich, D. H., Toracinta, E. R., Wei, H., Oglesby, R. J., Fastook, J. L., Hughes, T. J., 2004: Polar MM5 Simulations of the Winter Climate of the Laurentide Ice Sheet at the LGM*, *Journal of Climate*, **17**, 3415-3433

Cai, M., and M. Mak, 1990: Symbiotic relation between planetary and synoptic scale waves, *J. Atmos*. Sci., **47**, 2953–2968

Charney, J. G., 1947: The dynamics of long wave in a baroclinic westerly current, *J. Meteor.*, **4**, 125-162

CLIMAP Project, 1976: The surface of the ice-age earth, *Science*, **91**, 1131-1136,

Delworth, T. L., A. J. Broccoli, A. Rosati, R. J. Stouffer, V. Balaji, J. T. Beesley, W. F. Cooke, K. W. Dixon, J. Dunne, K. A. Dunne, J. W. Durachta, K. L. Findell, P. Ginoux, A. Gnanadesikan, C. T. Gordon, S. M. Griffies, R. Gudgel, M. J. Harrison, I. M. Held, R. S. Hemler, L. W. Horowitz, S. A. Klein, T. R. Knutson, P. J. Kushner, A. L. Langenhorst, H.-C. Lee, S. J. Lin, J. Lu, S. L. Malyshev, P.C. Milly, V. Ramaswamy, J. Russell, M. D. Schwarzkopf, E. Shevliakova, J. Sirutis, M. Spelman, W. F. Stern, M. Winton, A. T. Wittenberg, B. Wyman, F. Zeng, and R. Zhang, 2005: GFDL's CM2 global coupled climate models--Part 1: Formulation and simulation characteristics, *J. Climate*, **19**, 643-674

Donohoe, A., and D. S. Battisti, 2009: Causes of reduced North Atlantic storm activity in a CAM3 simulation of the Last Glacial Maximum, *J. Climate*, **22**, 4793–4808

Eady, E., 1949: Long waves and cyclone waves, Tellus, **1**, 33–52

Gates, W. L., 1976: Modeling the ice age climate, *Science*, **191**, 1138-1144

Justino, F., A. Timmermann, U. Merkel, and E. P. Souza, 2005: Synoptic reorganization of atmospheric flow during the Last Glacial Maximum, *J. Climate*, **18**, 2826–2846

Kutzbach, J. E., and P. J. Guetter, 1986: The influence of changing orbital parameters and surface boundary conditions on climate simulations for the past 18,000 years. *J. Atmos. Sci.*, **43**, 1726–1759

Laîné, A., Kageyama, M., Salas-Mélia, D., Voldoire, A., Rivière, G., Ramstein, G., Planton, S., Tyteca, S., Peterschmitt, J. Y., 2009: Northern hemisphere storm tracks during the last glacial maximum in the PMIP2 ocean-atmosphere coupled models: energetic study, seasonal cycle, precipitation, *Climate Dynamics*, **32**, 5, 593-614

Lau, N. C., 1978: On the three-dimensional structure of the observed transient eddy statistics of the Northern Hemisphere wintertime circulation, *J. Atmos. Sci.*, **35**, 1900-1923

Li, C., and D. S. Battisti, 2008: Reduced Atlantic storminess during Last Glacial Maximum: Evidence from a coupled climate model, *J. Climate*, **21**, 3561–3579

Lindzen, R. S., Farrell, B., 1980: A simple approximate result for the maximum growth rate of baroclinic instabilities, *J. Atmos. Sci.,* **37**, 1648-1654

Löfverström, M., Caballero, R., Nilsson, J., Messori, G., 2016: Stationary wave reflection as a mechanism for zonalizing the Atlantic winter jet at the LGM, *J. Atmos. Sci*., **73**, 3329–3342

Lorenz, E. N., 1979: Forced and free variations of weather and climate, *J. Atmos. Sci.*, **36**, 1367-1376

Manabe, S., Broccoli, A. J., 1984: Ice age climate and continental ice sheets: Some experiments with a general circulation model, *Annal. Glaciol*., **5**, 100-105

Manabe, S., Broccoli, A. J., 1985: The influence of continental ice sheets on the climate of an ice age, *J. Geophys Res,* **90**, 2167-2190

Oster, J. L., D. E. Ibarra, M. J. Winnickand, and K. Maher, 2015: Steering of westerly storms over western North America at the Last Glacial Maximum, *Nat. Geosci.*, **8**, 201–205

Peltier, W., 2004: Global glacial isostasy and the surface of the ice-age Earth: The ICE-5G (VM2) model and GRACE, *Annu. Rev. Earth Planet. Sci.,* **32**, 111–149

Rossby, C. G., 1939: Relation between variations in the intensity of the zonal circulation of the atmosphere and the displacement of the semi-permanent centers of action, *Journal of Marine Research*, **2**, 1, 38-55

Tarasov, L., Peltier, W. R., 2004: A geophysically constrained large ensemble analysis of the deglacial history of the North American ice-sheet complex, *Quat. Sci. Rev*., **23**, 359–388

Unterman, M. B. et al., 2011: Paleometeorology: High resolution Northern Hemisphere wintertime mid-latitude dynamics during the Last Glacial Maximum, *Geophys. Res. Lett*., **38**, L23702

Whittaker, L., Horn, L., 1981: Geographical and Seasonal distribution of North America cyclogenesis, 1958-1977, *J. Atmos. Sci.*, **109**, 2312-2322